Molecular Therapy
Oncology
Original Article

Smoldering oncolysis by foamy virus carrying CD19 as a CAR target escapes CAR T detection by genomic modification

Jason M. Tonne,[1] Karol Budzik,[1] Talia Fernandez Carrasco,[1,2] Landon Ebbert,[1] Jill Thompson,[1] Rebecca Nace,[1] Benjamin Kendall,[1] Rosa M. Diaz,[1] Stephen J. Russell,[1,2] and Richard G. Vile[1,3]

[1]Department of Molecular Medicine, Mayo Clinic, Rochester, MN 55905, USA; [2]Vyriad Inc, Rochester, MN 55901, USA; [3]Department of Immunology, Mayo Clinic, Rochester, MN 55905, USA

Chimeric antigen receptor (CAR) T cells have had limited success against solid tumors. Here, we used an oncolytic foamy virus (oFV) to display a model CAR target antigen (CD19) on tumors in combination with anti-CD19 CAR T cells. We generated oFV-Δ*bel2* and oFV-*bel2* vectors to test the efficiency and stability of viral/CD19 spread. While both viruses conferred equal CAR T killing *in vitro*, the oFV-Δ*bel2* virus acquired G-to-A mutations, whereas oFV-*bel2* virus had genome deletions. In subcutaneous tumor models *in vivo*, CAR T cells led to a significant decrease in oFV-specific bioluminescence, confirming clearance of oFV-infected tumor cells. However, the most effective therapy was with high-dose oFV in the absence of CAR T cells, indicating that CAR T clearance of oFV was detrimental. Moreover, in tumors that escaped CAR T cell treatment, resurgent virus contained deletions within the oFV-CD19 transgene, allowing the virus to escape CAR T elimination. Therefore, oFV represents a slow smoldering type of oncolytic virus, whose chronic spread through tumors generates anti-tumor therapy, which is abolished by CAR T therapy. These results suggest that further development of this oncolytic platform, with additional immunotherapeutic arming, may allow for an effective combination of chronic oncolysis.

INTRODUCTION

Immunotherapy offers a potential alternative for treating high-grade gliomas (HGGs), but has so far seen limited successes compared with the traditional modalities of surgery, radiation, or chemotherapy. Despite demonstrating tremendous benefits for hematologic malignancies,[1] success with chimeric antigen receptor (CAR) T cell therapy for HGG has been limited.[2–4] A potential modality is the use of oncolytic viruses (OVs) to target tumor cells resulting in direct oncolysis and subsequent immune stimulation, which can lead to increased trafficking of both innate immune cells and adaptive T cells to the tumor site. Therefore, several groups, including our own, have attempted to combine the immune-stimulatory properties of OV with CAR T cell therapy.[5] Additionally, OVs can be engineered to display a specific, unique CAR T cell target antigens (CAR_{TTA}) on the tumor cell surface during the process of oncolytic infection.[6–9] In this way, tumor cells can, in theory, be lysed directly by the OV and can display a CAR_{TTA} to allow for the killing of additional infected cells, which are insensitive to viral lysis. In this respect, it may be more effective to display the CAR_{TTA} from a viral vector that persists and spreads for a long period of time to allow adequate coverage of the tumor with the CAR_{TTA} before the administration of the CAR T cells.

Oncolytic foamy virus (oFV) has been described as a retroviral-based platform for oncolytic virotherapy,[10,11] offering cytolytic activity *in vitro* and oncolytic efficacy *in vivo* with broad tissue tropism,[12,13] natural tumor specificity,[10,14] and the ability to infect cells undergoing periods of quiescence.[10,15] Foamy virus requires cell division to integrate into the host genome. However, during cell quiescence, incoming foamy viruses accumulate near the centrosome inside the viral capsid, for up to 30- days, awaiting cell division.[15] This latency period provides oFV a significant advantage over TOCA-511,[16] the murine gammaretrovirus (gRV), by increasing the window of integration in slowly dividing cells. In addition, oFV possess several key properties over the gRV platform as vectors for human cancer therapy. These include induction of cell death by syncytia formation,[17] which non-pathogenic in natural hosts and in humans with zoonotic infection of FV,[18–20] and an integration profile favoring non-genic regions.[21]

Another unique feature of oFV is the presence of a ubiquitous internal promoter (IP) within the *env* gene that drives expression of two non-structural genes, *bel1* and *bel2*, which encode the proteins *trans*-activator protein (TAS) and BET, respectively. TAS activates the IP as well as the U3 long terminal repeat (LTR) of oFV. BET neutralizes the APOBEC3 cellular antiviral enzymes,[22–24] but is not essential for foamy virus infection.[25] Despite expression of BET, latent oFV genomes in zoonotically infected humans still contained G-to-A APOBEC3-signature mutations, and no difference in mutational load of wild-type foamy virus to foamy viruses lacking BET were detected.[22]

Received 14 February 2024; accepted 23 July 2024;
https://doi.org/10.1016/j.omton.2024.200852.

Correspondence: Richard G. Vile, Department of Molecular Medicine, Mayo Clinic, Rochester, MN 55905, USA.
E-mail: vile.richard@mayo.edu

In the current study, we tested the ability of oFV to establish a slow, spreading infection of solid tumors while simultaneously displaying a model CAR_{TTA}. Our hypothesis was that this strategy would enhance anti-tumor therapy by displaying CAR targets on those cells in which virus had spread, but that were resistant to oncolysis. The combined immune stimulatory effect of oncolysis plus CAR T cell tumor killing would then enhance endogenous anti-tumor immunity through both innate and adaptive immune responses, although we were unable to test this latter effect here in our immune-deficient models. Additionally, to test if BET could maintain genome stability by mitigating any potential mutations from APOBEC3 enzymes, we compared oFVs that either contained an intact, or deleted, *bel2* ORF with our CAR_{TTA} CD19. Based on these experiments we progressed a *bel2*-deleted oFV-CD19 virus (oFV-hCD19t) into therapeutic pre-clinical studies. oFV-hCD19t established an equilibrium between oncolysis and viral replication/spread, which allowed for chronic intra-tumoral viral persistence associated with modest anti-tumor therapy. Expression of the CAR_{TTA} was tightly coupled to viral persistence and intra-tumoral spread. Nonetheless, the administration of CAR T cells significantly decreased the therapeutic value of oFV oncolysis alone. Even with longer periods between oFV infection and CAR T cell administration, there was only a very small increase in therapy of the combinational therapy compared with virus alone. These data suggest future strategies in which a slow, simmering persistent oncolytic viral infection might be used to condition tumors for successful immunotherapy.

RESULTS

Bel2 intact and *Bel2* deleted oFV

Our goal was to test the hypothesis that the spread of an oFV engineered to express the hCD19t CAR antigen through an established tumor would allow significantly enhanced combinational therapy compared with oFV or CAR T cells therapy alone. Previously, Budzik et al.[10] generated an oFV-GFP infectious clone by cloning a T2A-GFP cassette in place of the *bel-2* open reading frame (ORF) generating the *bel2*-deleted oFV-GFP.[10] Here, we constructed a new infectious clone of oFV-GFP by replacing GFP with hCD19t (999 bp) to generate oFV-hCD19t (Figure 1A). Retention of intact BET protein in oFV has been reported to support better viral replication compared with ΔBET variants,[11] part at in part least through antagonizing the anti-viral activity of cellular APOBEC proteins.[22] Therefore, we also generated two additional infectious clones (oFV-*bel2*-GFP and oFV-*bel2*-hCD19t) in which the *bel2* ORF (encoding BET) was retained and the GFP or hCD19t transgenes were linked in frame with a T2A self-cleaving peptide (Figure 1A). This vector design is similar to a feline foamy virus vector published by Schwantes et al.,[26] where the transgene was inserted immediately behind the 3′ end of the *bel2* ORF in the U3 region of the U3 LTR. As a consequence, after reverse transcription, this intact *bel2*-T2A-transgene sequence will be transferred into the 5′ U3 region within the integrated provirus (Figures 1A and S1), thereby duplicating the sequence in both the 5′ and 3′ LTRs. Overall, this duplication significantly enhances the size of the proviral DNA of the *bel2*-intact, relative to the Δ*bel2* variants.

After viral expansion (as described in Budzik et al.[10,11]) and titration on BHK-U3 indicator cells (Figure S2), transgene expression from oFV-GFP, oFV-hCD19t, oFV-*bel2*-GFP, and oFV-*bel2*-hCD19t virus stocks was tested on U251 cells at three different multiplicities of infection (MOIs) (Figure 1B). At 72-h post-infection (p.i.), dose-dependent increases in GFP or CD19 expression were observed from both oFV-GFP and oFV-hCD19t, respectively (Figures 1B and 1C). Expression of both oFV-*bel2*-GFP and oFV-*bel2*-hCD19t was less efficient, at least at the 72-h p.i. time point (Figures 1B and 1C). Similarly, the oncolytic activity of both Δ*bel2* viruses across multiple MOIs was significantly higher than for the corresponding *bel2*-intact viruses (Figure 1D). These data show that the spread of oFV from Δ*bel2* viruses is more extensive than if expression of the *bel2* gene is retained.

oFV-expressed CD19 as a target for CAR T cell therapy

As the effector for oFV-expressed CD19 in tumors, we generated a second-generation human CD19 targeting CAR with a P2A self-cleaving peptide tethered to a GFP reporter (Figure 2A). Transduction efficiency of human T cells with this hCD19-P2A-GFP vector was typically between 40% and 60% of $CD3^+$ T cells (expressing both GFP and scFv-CD19) (Figure 2A). As before, by 72 h p.i., both oFV-GFP and oFV-hCD19t had spread more efficiently through U251-U3 indicator cells than had the corresponding oFV-*bel2* viruses (Figure 2B E:T ratio of 0:1, where luminescence indicates levels of oFV infection). Co-culture of the oFV-hCD19t, or oFV-*bel2*-hCD19t, infected target cells with anti-CD19 CAR T cells at increasing E:T ratios showed significant killing in both cases (Figures 2B and 2C) with oFV-bel2-hCD19t showing only a modestly increased significance compared with oFV-hCD19t. In contrast, no detectable killing was observed either upon co-culture of oFV-GFP, or oFV-*bel2*-GFP, infected target cells with anti-CD19 CAR-T cells, or upon co-culture of infected U251-U3 indicator target cells with un-transduced (UTD) T cells (Figures 2B and 2C). Consistent with the luminescence data, conditioned media collected 24 h after co-culture with CAR or UTD T cells showed significant CAR T cell activation (human interferon [IFN]-γ secretion) only from target cells infected with the oFV-hCD19t or oFV-*bel2*-hCD19t viruses, with no significant differences between viruses (Figure 2D). No human IFN-γ was secreted from cells infected with the oFV-GFP or oFV-*bel2*-GFP viruses, or from any infected target cells co-cultured with UTD T cells (Figure 2D). Very similar results were obtained in two additional pediatric HGG cell lines SF7761 and SOH (Figures 2E–2H). Thus, co-culture with anti-CD19 CAR T cells rapidly extinguished luciferase expression from the infected target cells after infection of SF7761 cells (which, in this case, express Firefly Luciferase intrinsically as a marker of cell survival rather than viral infection) with either oFV-hCD19t or oFV-*bel2*-hCD19t viruses but not with oFV-GFP or oFV-*bel2*-GFP viruses (Figures 2E and 2F where luminescence indicates levels of cell killing). Similarly, SOH cells engineered to express U3-luciferase (which, in this case now reflects viral infection rather than cell killing) showed significant decreases in luminescence only upon co-culture with anti-CD19 CAR T cells following infection with oFV-hCD19t or oFV-*bel2*-hCD19t viruses

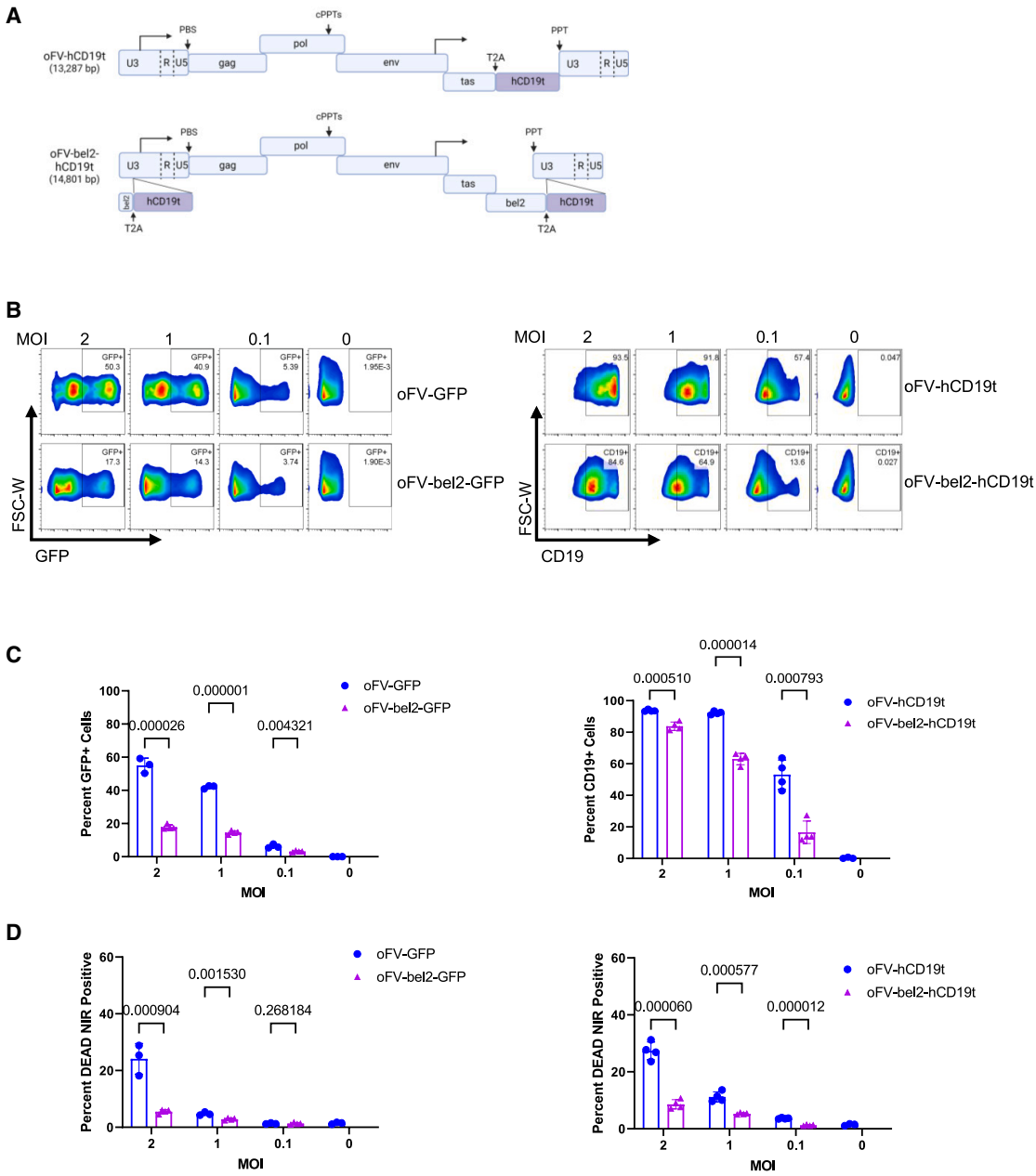

Figure 1. Bel2 Intact and Bel2 Deleted oFV

(A) Schematic representation of oFV used in this study: oFV-hCD19t and oFV-bel2-hCD19t. A truncated version of human CD19 (hCD19t) was cloned into oFV genome either in place of bel2 or linked to intact bel2 via T2A. (B) Flow cytometry plots of human U251 tumor cells infected with oFVs for 72 h at MOIs of 2, 1, or 0.1. Boxed region indicates GFP+ (left) or CD19$^+$ cells (right). (C) Quantification of percent GFP$^+$ (left) and CD19$^+$ (right) cells after oFV infection for 72 h at indicated MOIs. (D) Quantification of dead cells at 72 h p.i. with oFV-GFP (left) or oFV-CD19t (right). Data presented are from biological triplicates and shown as means ± SD. *p* values were determined in Prism using an unpaired t test.

(Figures 2G and 2H, where luminescence indicates levels of oFV infection).

Therefore, oFV expressing a CAR target antigen can both confer a *de novo* sensitivity to CAR T cell recognition and killing and lead to clearance of the virus from infected cell cultures.

Genetic stability of Δ*bel2* and *bel2* viruses

The value of oFV as a vehicle to spread expression of a CAR target antigen through a solid tumor depends in large part on the stability and coding integrity of the vector over time. Therefore, we determined the stability of oFV therapeutic transgenes when expressed from both Δ*bel2* or *bel2* viruses. Viruses were allowed to

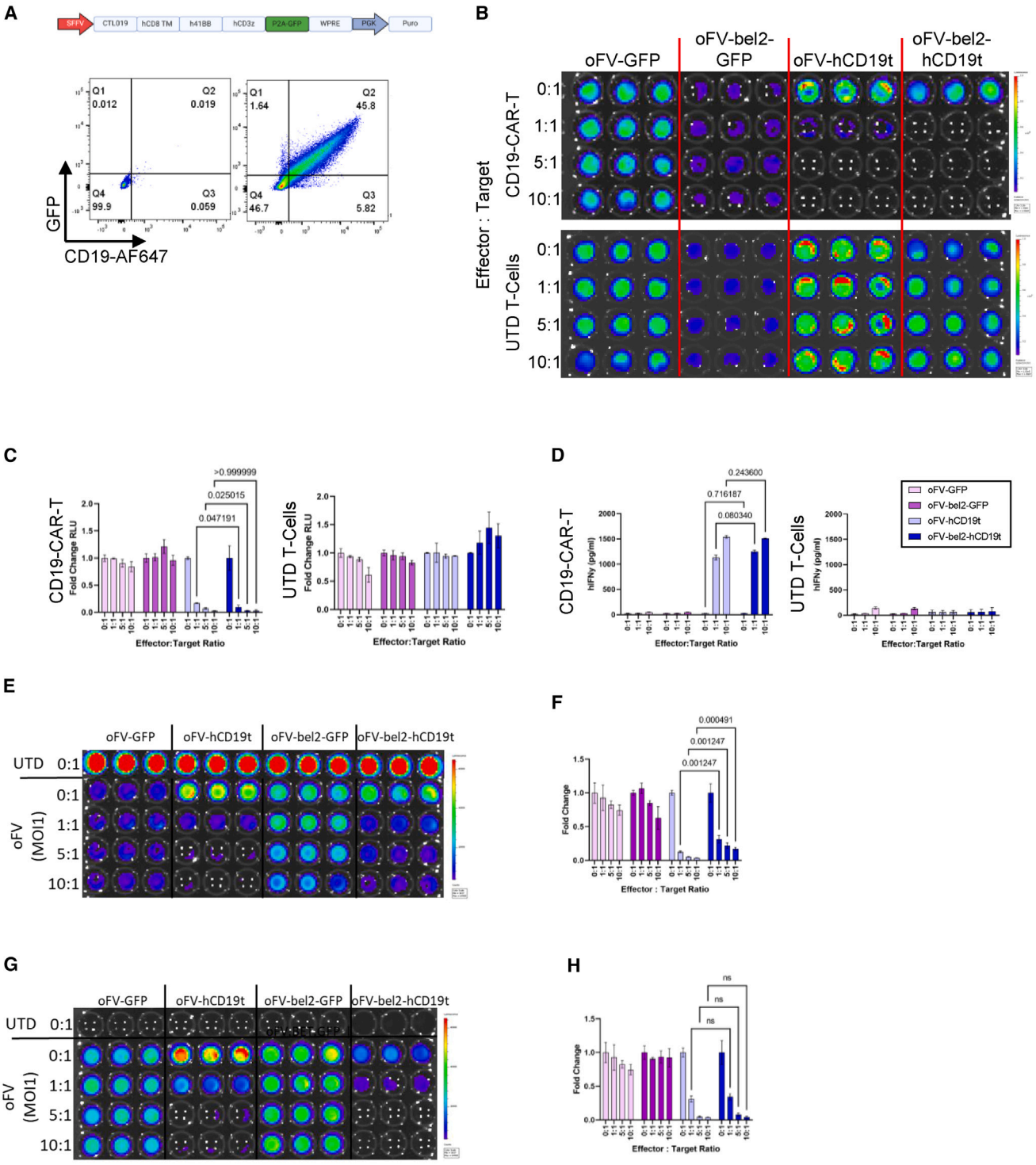

Figure 2. oFV-expressed CD19 as a target for CAR T cell therapy

(A) Schematic representation of our second generation human CD19 CAR-T lentivector and subsequent flow characterization of expression based on GFP reporter and detection of CD19 scFv with a recombinant CD19 protein bound to AF647 fluorophore. (B) Vital assay of U251-U3-F.Luc cells infected with oFVs at a MOI of 1 for 72 h before the addition of CD19 CAR-Ts (top) or UTD T-cells (bottom) at indicated ratios. The reaction was allowed 24 h co-culture before reading on luminometer. (C) Quantification of relative luminescent units (RLUs) and displayed as fold-change relative to the respective 0:1 control. *p* values were determined in Prism using an unpaired t test. (D) Human

(legend continued on next page)

spread through U251 cells infected at a very low MOI (0.01) and genomic DNA was analyzed at day 14 using primers specific for the appropriate transgenes (ORF) (Figure 3A), which amplify the entire ORF from the ATG to stop codons (Figure 3B). In addition, genomic DNA was analyzed for the oFV *env* gene to validate infection and the *bel-2* gene to validate each virus based on size (oFV-hCD19t, 1,231 bp; oFV-GFP, 951 bp; oFV-*bel2*-CD19 and oFV-*bel2*-GFP, 700 bp) (Figure 3B). Smaller than expected PCR bands for the transgene (ORF) (red asterisk) were observed, suggesting instability of virus structure through transgene truncation with passage *in vitro* (Figure 3B). TOPO-TA sequencing of purified PCR products did not reveal any significant difference in the number of total point mutations detected between infection with Δ*bel2* or *bel2* viruses (Figure 3C). Interestingly, there was a trend toward an increased frequency of deletions (of as much as 800 bp) in both oFV-CD19-expressing viruses, which was most pronounced in cells infected with oFV-*bel2*-hCD19t (Figure 3D). Long-term spread of both oFV-GFP and oFV-*bel2*-GFP was associated with deletions, although the size of these deletions was generally smaller, and they occurred at lower frequency, than with the CD19-expressing viruses (Figure 3D). Since the CD19-expressing viruses were larger than their GFP counterparts (oFV-*bel2*-GFP [14,592 bp] compared with oFV-*bel2*-hCD19t [14,801 bp]), it may be that this increased instability of the CD19-expressing viruses is associated with size limitations on the ability of oFV to replicate efficiently.

Virus stability and fidelity may also be associated with other factors, including sensitivity to anti-viral innate immune effectors such as expression of the APOBEC enzymes, against which the BET protein has been reported to be active.[22] Therefore, we investigated the mutational load imposed on oFV transgenes in the absence, or presence, of *bel2* using three-dimensional (3D) PCR. Since AT-rich DNA denatures at lower temperatures than GC-rich DNA, PCR amplification of AT-rich genomes will identify lower frequency variants that contain C-to-T or G-to-A mutations, which are the signature mutations associated with APOBEC3 mutational activity.[27] In Figure 3E, the red line indicates the lowest denaturation temperature at which plasmid DNA (non-mutated) are no longer amplified. PCR products generated at lower temperatures are indicative of mutated AT-rich templates. This 3D PCR analysis showed that at 15 days p.i. the oFV-GFP genome showed the highest amplification products at the lowest temperatures (down to 88°C), indicating the relatively highest rate of mutation among the viruses tested (Figure 3E). Sanger sequencing of gel extracted PCR bands amplified at 90°C for all viruses and plasmid controls showed a significantly higher rate of G-A mutation in oFV-GFP genomes compared with oFV-*bel2*-GFP genomes, consistent with the hypothesis that retention of *bel2* expression is associated with reduced anti-viral activity of APOBEC-induced viral mutation (Figures 3F and 3G). In an additional pediatric HGG cell line DIPG XIII, similar patterns were observed. In particular, significantly higher levels of deletions were once again observed in *bel2* retaining viral genomes compared with Δ*bel2* viruses (Figures 3H–3J). Thus, although multiple deletions were detected at both 7 and 15 days p.i. with oFV-*bel2*-GFP in DIPG XIII cells, many fewer deletions were detected in oFV-GFP viruses and not until later at day 15 p.i. (Figures 3H–3J).

Taken together these data show that an increased frequency of G-to-A mutations accumulated in oFV-Δ*bel2* genomes with time compared with *bel2* retaining genomes, consistent with BET inhibiting the anti-viral activity of APOBEC-induced viral mutation. In contrast, *bel2* retention was associated with increased levels of genome deletions.

In vivo spread of a CAR target antigen by oFV

We hypothesized that a slow spreading infection with oFV expressing a CAR target antigen would condition a tumor for subsequent CAR T cell therapy. However, since oFV is also oncolytic, it was unclear whether spread of the CAR target antigen would outpace the lysis of tumor cells expressing it. Therefore, to evaluate the intra-tumoral spread and stability of hCD19t (as a target for anti-CD19 CAR T cells) by oFV with, or without, *bel2*, established U251-U3-indicator tumors were injected with two doses of 5×10^5 IU oFV-hCD19t or oFV-*bel2*-hCD19t (Figures 4A–4E). Although we were technically unable reliably to assess CD19 levels by flow cytometry, both viruses induced an increase in total radiance (indicative of viral infection) from days 9 to 16 after virus injection (Figures 4A and 4B). However, there was no significant difference in radiance between the Δ*bel2* and *bel2* containing oFV (Figure 4B).

Complete amplicon sequencing of a 450-bp segment of hCD19t recovered from these tumors showed only a very low proportion of G-to-A mutations, as well as a few small deletions, in the CD19 transgene from Δ*bel2*-hCD19t-infected tumors relative to the same 450-bp segment sequenced from plasmid DNA as a control (Figures 4C–4E). In contrast, CD19 sequenced from tumors infected with the oFV-*bel2*-hCD19t virus contained significantly more deletions, including a dominant 44-bp deletion with an additional G-to-A mutation (tumor #13) (Figure 4E).

These data indicate both viruses spread effectively *in vivo*, that loss of *bel2* was not associated with very high mutational loads, and that retention of *bel2* generated increased frequency of deletions in the transgene.

IFN-γ production measured by ELISA in conditioned media after 24 h of co-culture with each indicated oFV-infected U251-U3 cells and CAR-Ts (left) or UTD T-cells (right). DIPG SF7761-F.Luc. (E) and DIPG SOH-U3 (G) cells were seeded 50,000 cells/well in a 96-well plate and infected at a MOI of 1 with the indicated oFVs. After 72 h, CD19 CAR-T were added at indicated effector to target ratios. Co-culture was allowed 24 h before reading luminescence. Quantification of RLUs for SF7761-F.Luc (F) and DIPG SOH-U3 (H), displayed as fold-change relative to the respective 0:1 control. Data presented are from biological triplicates and shown as means ± SD. *p* values were determined in Prism using an unpaired t test.

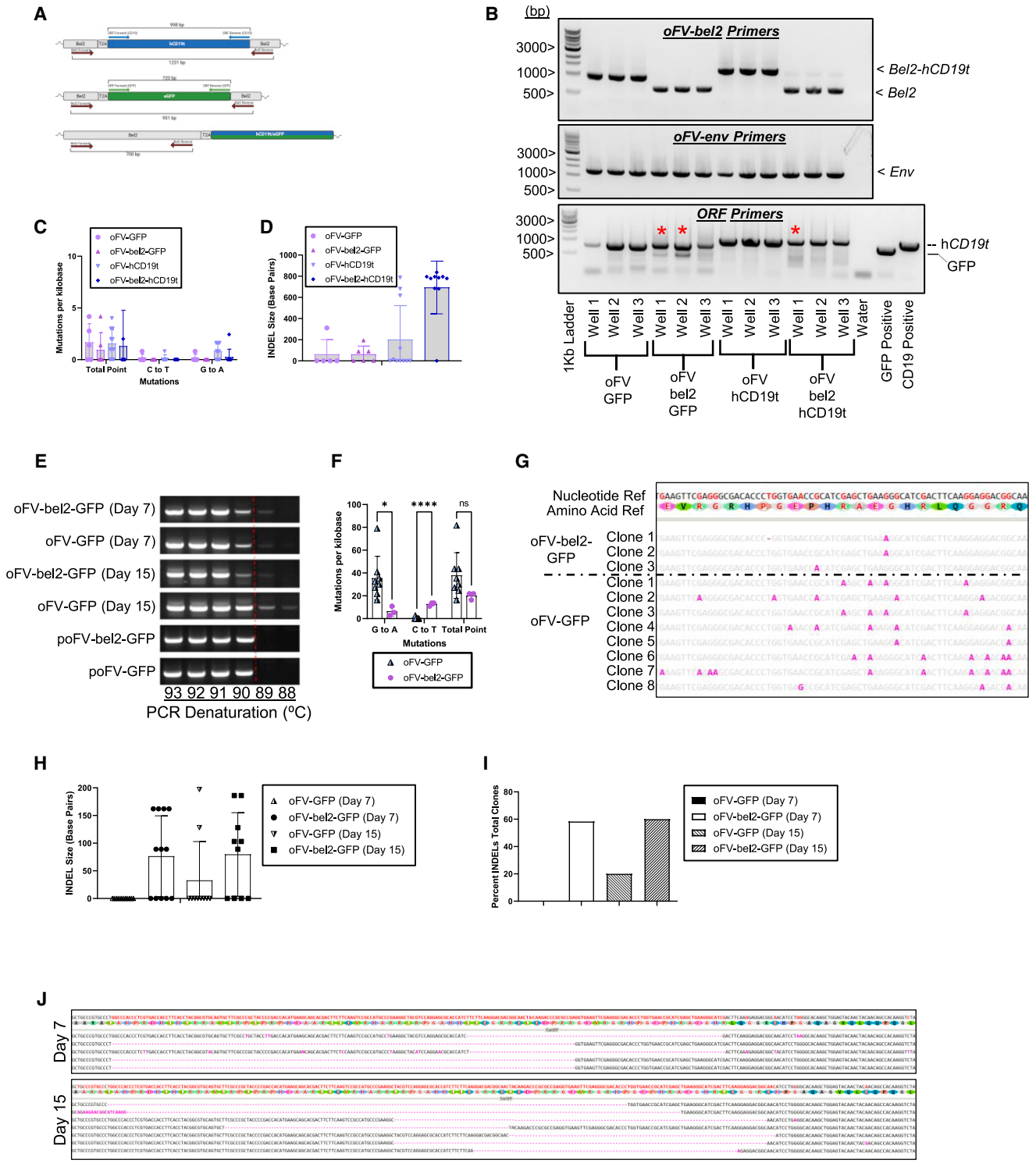

Figure 3. Genetic stability of Δbel2 and bel2 viruses

(A) Schematic representation showing primer binding sites and expected amplicon size on the oFV genome. Bel2 primers indicated by red arrows, hCD19t primers indicated by blue arrows, and eGFP indicated by green arrows. (B) Agarose gels showing PCR amplification of oFV genes. Briefly, U251 cells were infected with MOI 0.01 at Day 0, cells were passaged every 2 days and virus allowed to infect/spread up to Day 14 p.i. U251 cells were collected, and genomic DNA was collected at Day 14 (B). PCR was conducted using primers to oFV-Bel2, oFV-ENV and GFP/CD19 specific ORF primers. Positive controls (poFV-GFP and poFV-CD19 plasmid); Water, no-template

(legend continued on next page)

oFV therapy is superior to combinatorial oFV and CAR T cell therapy

Based on the mutational data of Figure 4, we took the oFV-hCD19t forward for combinational *in vivo* therapy with oFV-hCD19t and CAR T cells to decrease the occurrence of large-scale deletion mutation in the transgene. As a surrogate marker for the spread of the CD19 CAR target through tumors, we used U251-U3-indicator tumors. These cells have a stably integrated oFV U3 LTR promoter upstream of firefly luciferase and mCherry, so that luciferase and or mCherry expression reflects levels of virus spread. U251-U3-indicator tumors growing in NSG mice were injected with 1×10^7, 6.6×10^6, or 3.3×10^6 IU of oFV-hCD19t intra-tumorally and then at day 11 treated intravenously with either human T cells (UTD, 5×10^6 cells/mouse) or human anti-CD19 CAR-T at 5×10^6 cells/mouse (Figure 5A). As before (Figures 4A and 4B), virus spread was observed in all groups before CAR T cell treatment (day 7) (Figure 5A). Virus spread increased progressively in mice treated with UTD human T cells (days 14–23) (Figures 5A and 5B) before reaching a plateau (days 23–36) (Figures 5A and 5B). In contrast, treatment of oFV-hCD19t injected tumors with anti-CD19 CAR T cells induced highly significant loss of virus in the tumors at all viral treatment doses (Figures 5A and 5B) (days 7–29).

We observed that those mice in which initial infection with oFV-hCD19t was inefficient by day 7 generally reached endpoint for the study (tumor $\geq$1.2 cm) more rapidly than mice in which robust viral infection was seen by day 7 (Figure 5A). These observations suggested that treatment with oFV-hCD19t alone (in the absence of supportive CAR T cell therapy) was an effective anti-tumor treatment, consistent with the oncolytic nature of this virus.[10,11] This is consistent with the plateauing of virus spread through tumors in the absence of CAR T cell treatment (Figures 5A and 5B), reflecting the establishment of an equilibrium between viral replication, spread, and oncolysis.

Our initial hypothesis was that oFV-mediated spread of the CD19 CAR target antigen would allow for a combinatorial efficacy of oncolysis by the oFV plus additional cell killing by anti-CAR T cells targeting transduced, but virus-resistant, tumor cells. However, the most effective therapy was achieved with a high dose oFV (1×10^7 IU/mouse) and UTD human T cells (Figures 5C and 5D). In contrast, all therapies in which CAR T were added to virus-infected tumors were less significantly therapeutic compared with PBS treatment alone (Figures 5C and 5D), indicating that CAR T cell-mediated clearance of oFV-hCD19t was detrimental compared with the ongoing oncolytic activity of the virus alone.

oFV delivers CAR T cell target to tumors

As expected, mice treated with no virus and no T cells had no intra-tumoral T cell infiltration and no CAR T cells were detected at endpoint (tumor $\geq$1.2 cm) (Figure 5E). However, a trend was observed toward increasing levels of intra-tumoral CAR T cells in endpoint tumors associated with increased initial viral dose (Figures 5E and 5F). Since these measurements were taken long after the therapy was administered, it is likely that the trends observed in Figures 5E and 5F would have been more pronounced/significant had we measured immune infiltrations at earlier time points after therapy. Nonetheless, the fact that these trends were still in evidence at these later time points suggest that viral/CD19 load positively correlated with CAR T infiltration.

Viral infection was reproducibly detected in tumors from mice treated with oFV-hCD19t and UTD T cells (Figures 5G and 5H) (U3-cherry positive cells). Infection largely correlated with CD19 expression (Figure 5H) and was associated with $CD3^+$ T cell infiltration (Figure 5G). As expected, mice treated with PBS and PBS showed no viral infection and relatively widespread viral infection was observed throughout tumors treated with oFV-hCD19t and UTD T cells (Figures 5I and S3). Interestingly, however, those mice treated with both oFV-hCD19t and anti-CD19 CAR T cells and which died earliest from tumor burden (e.g., mouse #2 in the 6.6×10^6 treated group) were almost completely devoid of virally infected cells at endpoint, confirming once again that CAR T cell therapy was extremely efficient at clearing the majority of virally infected, CD19-expressing tumor cells.

Taken together, the data of Figure 5 show that it was preferable to let infection with a spreading virus, with low level oncolytic activity, persist rather than remove the infection by treatment with CD19-targeting (and therefore virus-targeting) CAR T cells.

oFV persistence is linked to the loss of CAR target antigen expression

Mice treated with both oFV-hCD19t and anti-CD19 CAR T cells, and which died earliest from tumor burden, showed significantly less oFV infection based on U3-F.Luc (days 14–29) (Figure 5). In mice that

control; 1-kb Ladder, DNA Standard. (C-D) The first biological rep of each group, Well#1, for the ORF-specific PCR products (GFP & CD19) was gel extracted and cloned into TOPO-TA. Up to 12 clones were selected/group and sanger sequenced. Total point mutations were quantified, as well as C-to-T and G-to-A mutations (C). (D) Shows base pair size of deletions identified in each TOPO clone. Individual points represent each clone, bar graph represents mean ± SD of group. (E-J) DIPG-XIII cells infected at low MOI 0.01 on Day 0. Virus allowed to spread for 15-days in culture. (E) Genomic DNA isolated at days 7 and 15 p.i. 3D-PCR was conducted against GFP transgene at different denaturation temperatures from 93C to 88C. Red-line represents threshold where PCR fails in healthy, bottom two contain unmutated plasmid control samples. (F) PCR bands from the 90C lane for each group were gel extracted and Topo cloned. The bar graph shows summary of total point mutations identified in sanger sequencing is represented as the means ± SD. The *p* value was determined using an unpaired two-tailed t test. (G) Representative image of sequencing alignment to GFP reference sequence. Three clones were obtained for oFV-bel2 and eight clones obtained for oFV-Δbel2. Point mutations are highlighted in red. (H-J) Summary of deletions found in Topo clones after sequencing. (H) Individual deletion size per clone represented as means ± SD. (I) Mean of all clones per group that have deletions in sequence. (J) Representative image of sequencing alignment to GFP reference sequence. Five clones were obtained for oFV-bel2 Day 7 and seven clones obtained for oFV-bel2 Day 15. Point mutations are highlighted in pink. Deletions are denoted by a dash or hyphen.

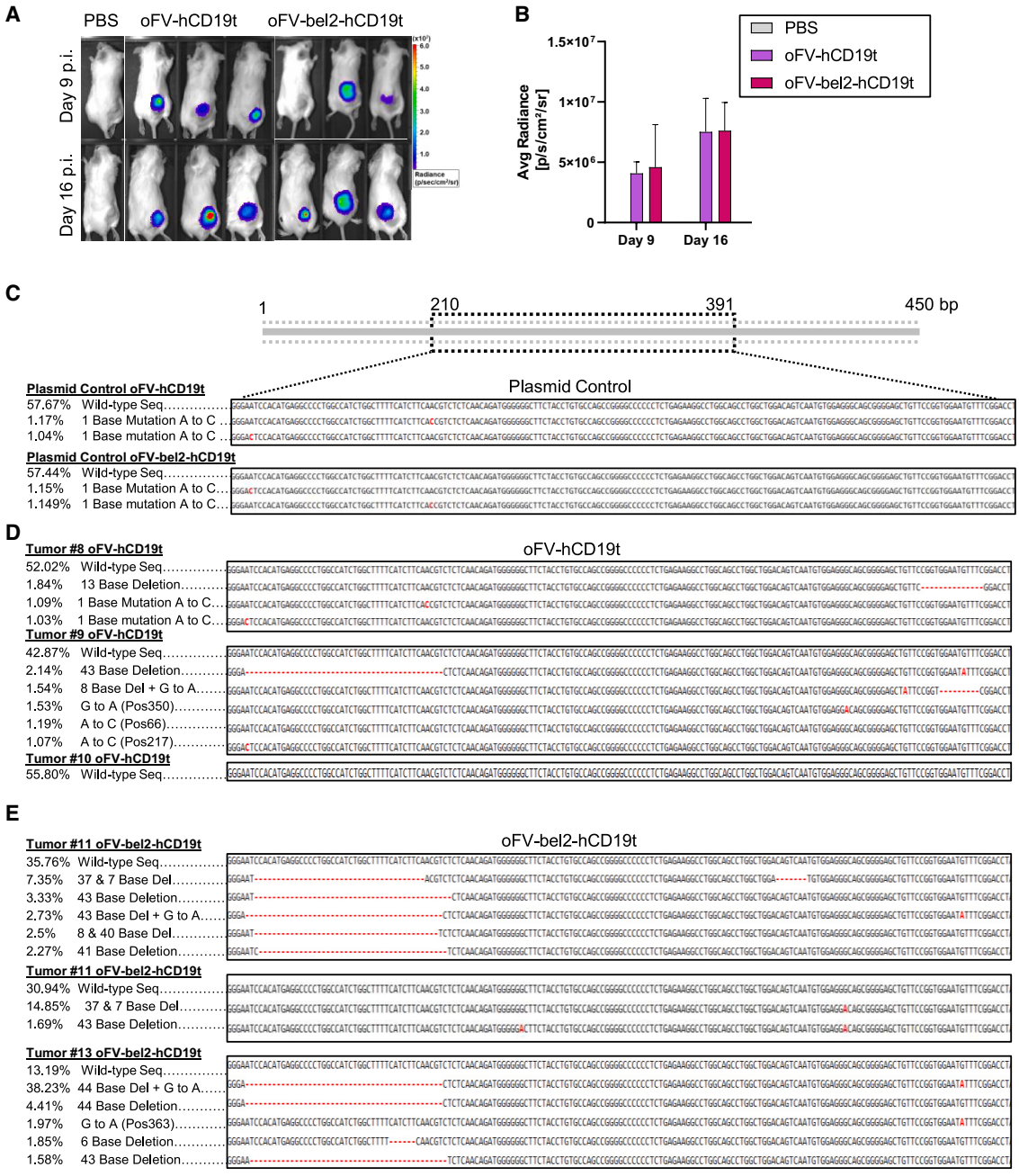

Figure 4. *In vivo* spread of a CAR target antigen by oFV

(A) IVIS Xenogen bioluminescence imaging of subcutaneous indicator U251-U3-mCherry-U3-Luc tumors expressing firefly luciferase in response to oFV infection. Tumors were directly injected with 2 doses of 5e5 IU (1e6 IU total) of either oFV-hCD19t, oFV-bel2-hCD19t or PBS control. Mice were imaged at days 9 and 16 p.i. (B) Averaged radiance (p/s/cm2/sr) of the IVIS Xenogen bioluminescence represented as the means ± SD. (C–E) Complete amplicon sequencing of oFV derived hCD19t transgene from U251 subcutaneous tumors shown in (A). DNA was isolated from tumors at day 30. Primers containing next-generation sequencing adaptors were designed to amplify a 450-bp region of hCD19t. Representative summary of overall analysis for each tumor showing percent of unique sequences obtained for plasmid controls (C), oFV-hCD19t (D), and oFV-bel2-hCD19t (E). Point mutations are high-lighted in red; deletions are highlighted with a red hyphen.

controlled tumor for longer, viral clearance was followed by a recurrence of the signal of viral infection (days 29–36), suggesting that viral evolution was occurring *in vivo* to escape CAR T cell-mediated viral/CD19 clearance. Using *bel2* primers that flank the inserted T2A-hCD19t gene, CD19 transgene was detected in six of eight endpoint tumors from mice treated with oFV-hCD19t and UTD T-cells and

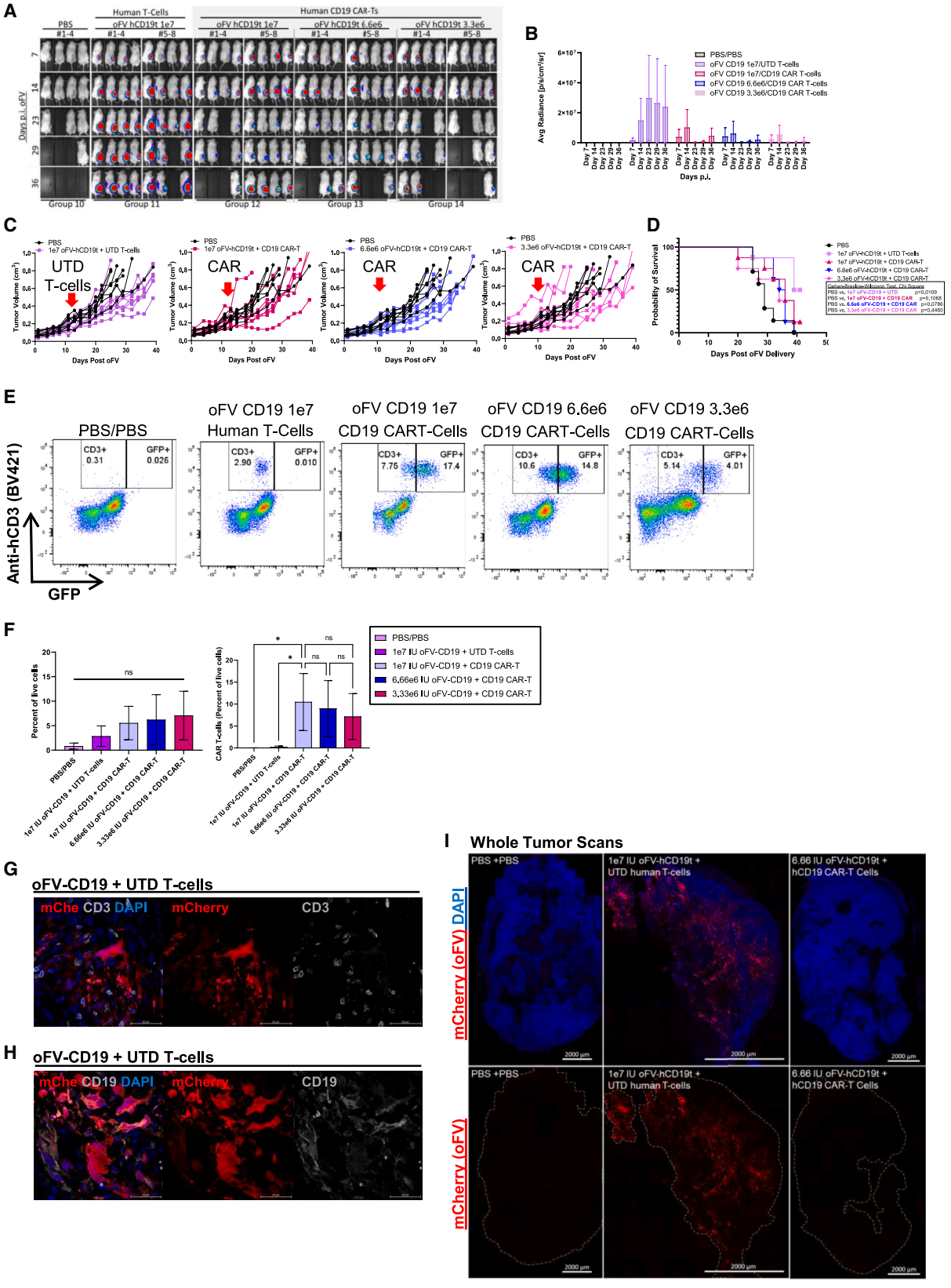

(legend on next page)

the oFV *env* gene was similarly detected in seven of eight tumors (Figure 6A). The majority of these PCR bands were of the correct size consistent with the positive plasmid control (Figure 6A). CD19 amplicon was detected in six of seven endpoint tumors from mice treated with oFV-hCD19t and CAR T cells and the oFV *env* gene was detected in all seven of these tumors (Figure 6B). However, unlike the case with UTD treatment, only one of seven of the CD19 amplicons was full length and of the expected size, suggesting a high frequency of deletions of the CAR target in these escaped viruses (Figure 6B). Cloning and sequencing of these bands showed that both sets of tumors contained mutations at a rate of fewer than 5 mutations/kb, most of which were G-to-A (Figures 6C and 6D). Deletions were present in viruses from within individual tumors treated with oFV-hCD19t and UTD T cells at a mean frequency of 29.51% per tumor, despite these not being visible on the agarose gel (Figure 6C). Nonetheless, there was a clear trend toward a higher frequency of deletions in the viruses recovered from mice with tumors treated with oFV-hCD19t and CAR T cells (Figures 6C–6E). Consistent with the hypothesis that retention of the CAR target CD19 transgene was associated with both diminished tumor therapy and viral persistence in the tumor, the mouse bearing tumor 12.3 (treated with oFV-hCD19t and CAR T cells) had an intact CD19 transgene by both agarose gel and sequence analysis and reached endpoint with a large tumor rapidly by only day 20 p.i. with virus (Figures 5 and 6B–6E).

We next conducted qPCR on the tumor DNA to determine levels of oFV infection based on *T2A-hCD19t* sequence and oFV-*env* (Figures 6F–6H). The mean levels of T2A-hCD19t were more a 1,000-fold higher in oFV-hCD19t and human T cells group (PBS/PBS group mean 0.108, oFV-hCD19t + Human T cells group mean 130.841, oFV-hCD19t + hCD19 CAR T group mean 5.594) (Figure 6F). oFV-*env* gene levels were very similar to *T2A-hCD19t* (Figure 6G). To determine relative intact retention of the CD19 transgene in oFV, we determined the ratio of env to CD19 (as in Budzik et al.[11]), data that suggested that addition of CAR T cells increased the loss of hCD19t transgene, though the results did not reach significance (Figure 6H).

Overall, these data show that the application of CAR T cell therapy enforced a high rate of viral mutation mainly through deletions of the CD19 gene.

Longer viral spread minimally enhances CAR T therapy

Our data show that the premature removal of CD19-expressing, oFV-infected cells was more detrimental than allowing a slow spreading infection with oFV alone to persist (Figure 5). Therefore, we hypothesized that leaving viral infection to spread for longer may spread CD19 expression more widely through the tumor than under the conditions of Figure 5 and enhance the therapeutic value of oFV/CAR T combinatorial treatment. U251-U3-indicator tumors were therefore allowed to develop until a size of 0.5 cm in diameter before being injected IT with PBS, oFV-GFP, or oFV-hCD19 t at 1×10^7 IU/mouse. 35 days p.i., (instead of day 7 p.i. as in Figure 5) mice received IV human anti-CD19 CAR T cells at 5×10^6 cells/mouse (Figure 7A). As before, before treatment with CAR T cells progressive spread of both oFV-GFP and oFV-hCD19t infection was observed through the tumors (Figure 7A). Tumors treated with oFV-GFP continued to show increased spread of the virus as detected by U3-directed luminescence following CAR T cell administration (Figures 7A and 7B days 35–42) which plateaued and started to decrease as mice succumbed to large tumors. In contrast, day 35 treatment with anti-CD19 CAR T cells induced very rapid loss of viral infection, as quickly as four days post-CAR T delivery. Viral clearance appeared to be almost complete, with the exception of one mouse, until the mice succumbed to tumor (Figures 7A and 7B days 35–48). Treatment with both oFV-GFP and oFV-hCD19t were, again, significantly better than control PBS treatment, confirming their value as oncolytic agents (Figures 7C and 7D). In addition, under these circumstances of a longer period between virus infection and CAR T cell administration, treatment with the combination of oFV-hCD19t with anti-CD19 CAR T was just significantly more therapeutic than oFV-GFP with anti-CD19 CAR T, suggesting that intratumoral spread of CAR target antigen may combine with CAR T therapy to improve on oFV alone, although this improvement was clearly very modest (Figure 7D). Interestingly, we observed a discrepancy between some tumor sizes and mouse survival. Several mice treated with oFV-hCD19t with anti-CD19 CAR T had generally larger tumors at early time points than mice treated with oFV-GFP and yet survived longer (Figures 7A, 7C, and 7D). In this respect, the earlier death of some of the mice in the oFV-GFP group (with smaller tumors than in the oFV-hCD19t with anti-CD19 CAR T group) was due to the increased weight loss associated in some mice with metastases appearing in the axillary lymph nodes. Mice in the oFV-hCD19t with anti-CD19 CAR

Figure 5. oFV therapy is superior to combinatorial oFV and CAR T cell therapy

(A) IVIS Xenogen bioluminescence imaging of NSG mice bearing subcutaneous indicator U251-U3-mCherry-U3-Luc tumors expressing firefly luciferase in response to oFV infection. Tumors were directly injected with oFV-hCD19t to achieve indicated doses (PBS control, 1e7, 6.6e6, or 3.3e6 IU oFV/mouse; n = 8/group). Mice were imaged at days 7, 14, 23, 29, and 36 p.i. At day 11 p.i., mice received either PBS, UTD human T-cells (5e6/mouse) or human anti-CD19 CAR-T cells (5e6/mouse) were administered IV. (B) Averaged radiance (p/s/cm^2/sr) of the IVIS Xenogen bioluminescence represented as the means ± SD. (C) Individual tumor volumes (cm^3) per group. CAR-T cells delivery time denoted by red arrow. (D) Survival of the NSG mice bearing U251-U3-tumors after combinational therapy with oFV and CD19 CAR-T. p values determined by the Gehan-Breslow-Wilcoxon test. (E) Upon endpoint, tumors were extracted from mice and dissociated into single cells for flow analysis. Flow analysis was done using FlowJo software with size, single cell, and zombie NIR gating. Plots show human CD3 (y axis) and GFP (x axis) to identify the human T-cells and CAR-T in tumors. (F) CD3$^+$ and CD3$^+$/GFP$^+$ (CAR-Ts) cells were quantified in the tumor and represented as mean ± SD. The p value was determined using an unpaired two-tailed t test. (G and H) Confocal imaging (40× objective) of tumor sections showing mCherry (red) fluorescents and stained for either anti-human CD3 (G; gray) or anti-human CD19 (H, gray) with DAPI nuclear staining (blue). (I) Whole-tissue slide scans conducted at 20× objective showing distribution of oFV-activated mCherry (red) fluorescents through tumor sections of PBS/PBS, oFV-CD19/T cell, and oFV-CD19/CD19 CAR-T treated tumors. Scale bars at 2000um.

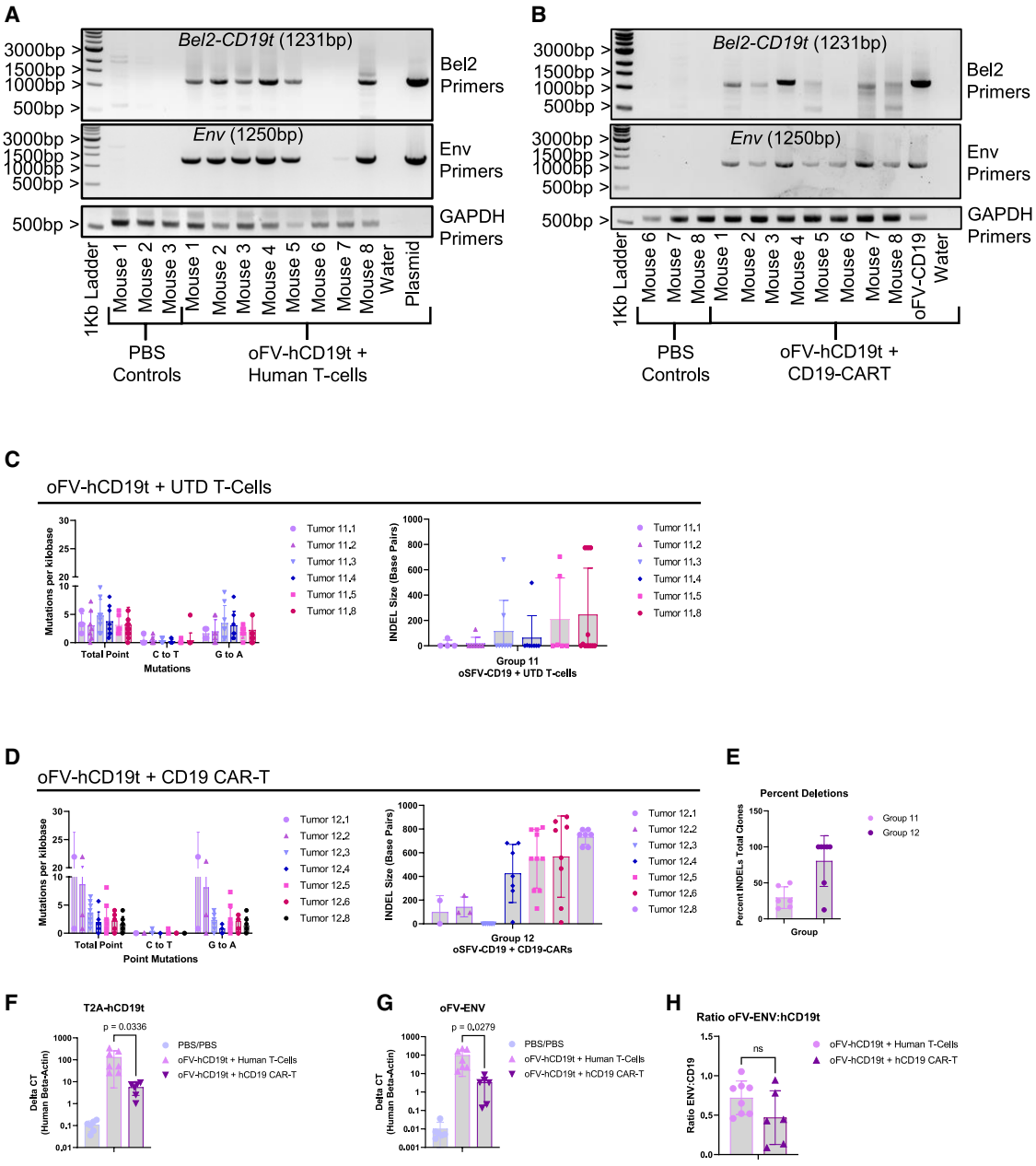

Figure 6. oFV persistence is linked to loss of CAR Target antigen expression

(A and B) Agarose gels showing PCR amplification of oFV specific genes with GAPDH housekeeping gene. Briefly, DNA was extracted from subcutaneous tumors shown in Figure 5A (1e7 IU oFV-CD19/human T cells [A] and 1e7 IU oFV-CD19/CD19 CAR-T cells [B]) and PCR was conducted using primers to oFV-Bel2, oFV-ENV, and GAPDH housekeeping control. Positive controls (poFV-CD19 plasmid [A] and oFV-CD19 virus [B]). Water, no-template control; 1-kb ladder, DNA standard. (C–E) Bel2 PCR products (A, top, and B, top) were gel extracted and cloned into TOPO-TA. Up to 12 clones were selected per group and Sanger sequenced. Total point mutations were quantified, as well as C-to-T and G-to-A mutations (C and D, left). Average deletion size was quantified in each TOPO clone (C and D, right). Individual points represent each clone, bar graph represents mean ± SD of group. (E) Shows percent of all Topo clones per tumor that contained a deletion represented as mean ± SD of group. (F–H) QPCR on DNA isolated from tumors of PBS/PBS, oFV-hCD19t + Human T-Cells, and oFV-hCD19t + hCD19 CAR-T. Showing Delta CT values normalized to human beta-actin. Each data point indicates an individual tumor. Bar graph represents mean ± SD of group. p values were determined in Prism using an unpaired t test.

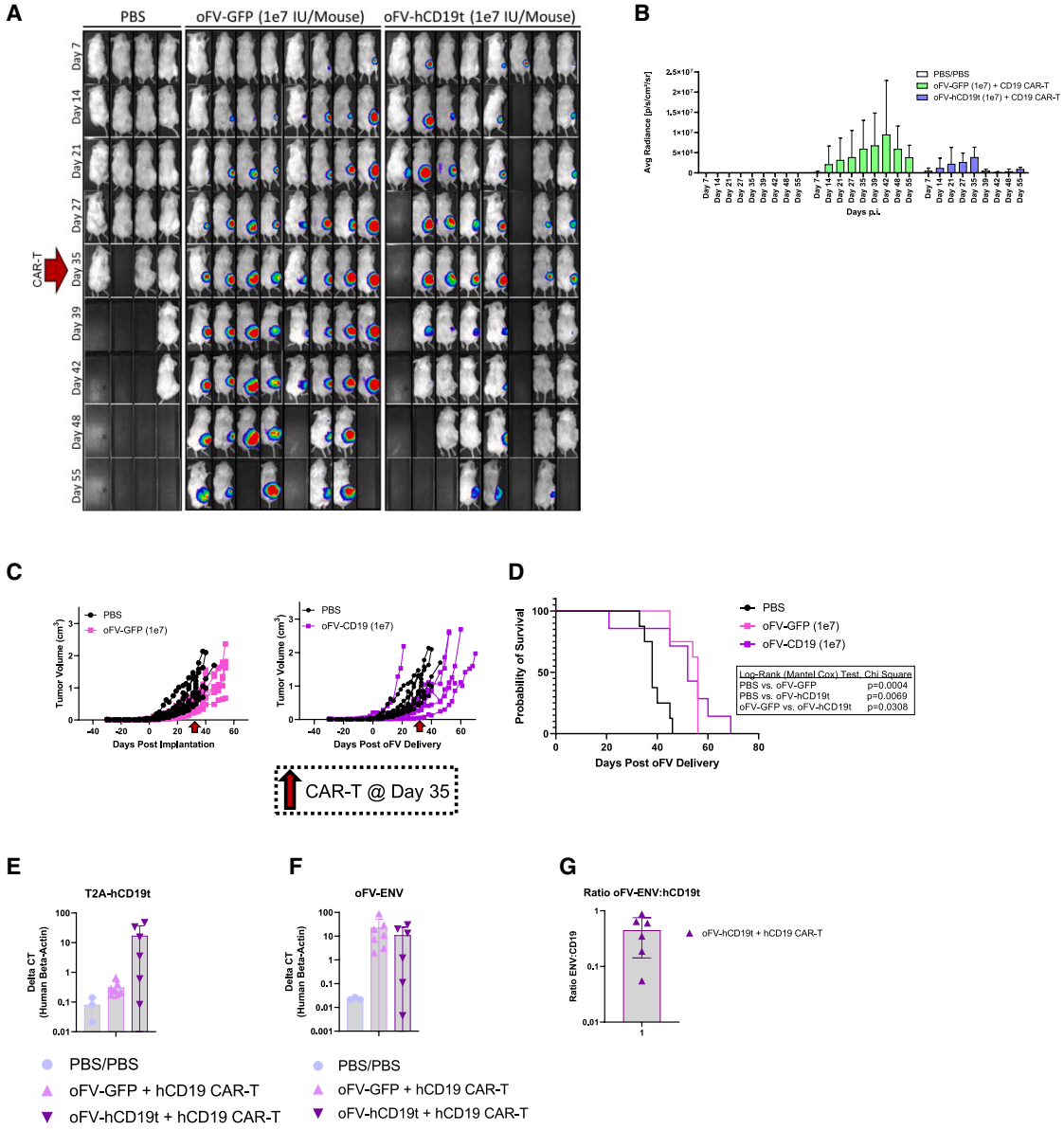

Figure 7. Longer viral spread minimally enhances CAR T therapy

(A) IVIS Xenogen bioluminescence imaging of NSG mice bearing subcutaneous indicator U251-U3-mCherry-U3-Luc tumors expressing firefly luciferase in response to oFV infection. Tumors were directly injected with two rounds oFV-GFP (5e6 IU/mouse) and oFV-hCD19t (5e6 IU/mouse) over 2 days to achieve a final dose of 1e7 IU/mouse (PBS/PBS, oFV-GFP, oFV-hCD19t; $n = 8$/group). Mice were imaged at days 7, 14, 21, 27, 35, 39, 42, and 48 p.i. At day 35 p.i. (red arrow), mice received either PBS or human anti-CD19 CAR-T cells (5e6/mouse) were administered i.v. (B) Averaged radiance (p/s/cm^2/sr) of the IVIS Xenogen bioluminescence represented as the means ± SD. (C) Averaged tumor volume (cm^3) per group shown as mean ± SD. CAR-T cells delivery time denoted by red arrow. (D) Survival of the NSG mice bearing U251-U3-tumors after combinational therapy with oFV and CD19 CAR-T. *p*-values determined by Gehan-Breslow-Wilcoxon test. (E–G) QPCR on DNA isolated from tumors of PBS/PBS, oFV-GFP + hCD19 CAR-T, and oFV-hCD19t + hCD19 CAR-T. Showing Delta CT values normalized to human beta-actin. Each data point indicates an individual tumor. Bar graph represents mean ± SD of group.

T group did not experience these weight loss issues and were euthanized predominantly on the basis of tumor size endpoints. In addition, given the correlative data showing a trend toward increased T cell infiltration of CAR and virus treatment, the larger size of the tumors in the oFV-hCD19t with anti-CD19 CAR T group compared with the oFV-GFP group is likely to reflect pseudo-progression, wherein tumor size reflects (tumor plus infiltration of CAR T) rather than more aggressive tumor growth *per se*.

As in Figures 6F–6H, qPCR on tumor DNA (Figures 7E–7G) indicated high levels of loss of the *T2A-hCD19t* gene compared with the env gene after CAR T administration (Figures 7E–7G).

DISCUSSION

We have observed that oFV spreads relatively slowly through established tumors with a low level of oncolysis, suggesting that many tumor cells are not efficiently killed even though they are infected.[10,11] We reasoned, therefore, that by expressing a CAR target antigen from the oFV platform, we would enhance anti-tumor therapy by displaying CAR targets on those cells in which virus had spread but were resistant to oncolysis. Our hope was that this combination of slow spread, basal level of oncolysis, and CAR target display would, therefore, enhance therapy over and above that induced by oFV alone. Here we show that oFV was indeed capable of spreading through tumors and conferring expression of the CD19 CAR target antigen; however, to our surprise, it was therapeutically more valuable to leave the virus alone to spread than to administer CAR T cells and clear virally infected cells.

Our work here is not the only approach for using an OV to deliver CAR_{TTA}s to tumors. Park et al.[6] used oncolytic vaccinia virus to deliver hCD19t (OV19t) to tumors in immunocompetent mice for combinational therapy with CD19 CAR T cells in which they showed promising results of reduced tumor burden, greater survival rates, and increased immune infiltration of $CD3^+$ and $CD8^+$ cells in tumors receiving both OV19t and CAR T cells. Additionally, Aalipour et al.[8] used a modified vaccinia virus to deliver CD19 CAR antigen in an immunocompetent B16 model, which led to significant reductions in tumor volume when compared with virus alone or CAR T cells alone. Tang et al.[9] also used combinational therapy with a tumor-specific promoter-driven oncolytic adenovirus expressing hCD19 in xenograft mouse models. Finally, Liu et al.[7] used oncolytic herpes simplex virus (oHSV) to deliver the dual CAR T cell antigens, CD19 and BCMA, with the T cell chemokine CCL5 to xenograft tumors in immune-deficient mice. This polycistronic oHSV labeled numerous different tumor types with CD19, BCMA, and CCL5 and allowed for CAR T cell targeting of heterogeneous tumors.

We constructed oFV vectors in which expression of the *bel2* gene was either retained or deleted. Although BET has many proposed roles, including regulating viral latency, reduction of lysis, and decreased structural gene expression (gag, pol, and env),[28] we investigated whether the reported ability of BET to antagonize anti-viral cellular responses, such as those mediated by APOBEC proteins, would affect the efficiency of the oFV platform.[22] Design of our *bel2* retaining vector was similar to Schwantes et al.[26] (2002) in which the transgene is inserted in the 3′ end of the *bel2* ORF within the U3 region of the U3 LTR. As a consequence, this sequence is duplicated in both 5′ and 3′ LTRs, significantly enhancing the size of the pro-viral DNA of the *bel2*-intact, relative to the Δ*bel2* variants. In contrast, our Δ*bel2* viruses were cloned in-frame with the *bel2* ORF and expressed as a result of the alternative splicing pathway that normally generates BET (Figure S1) without any inclusion within the U3 region of the 3′ LTR. The data of Figures 1 and 2 show that the Δ*bel2* oFV vectors showed significantly greater expression and cytotoxicity in short-term assays (Figures 1B and 1C) and that their spread was more extensive than if expression of BET was retained. Since retention of *bel2* clearly increases the size of the replicating virus genome it may be that these effects are associated simply with size constraints imposed upon the virus for viral genome packaging. Alternatively, it may be that retention of the *bel2* ORF within the U3 of the 3′LTR reduces the efficiency of replication when that cassette is transferred into the 5′LTR. Overall, the improved efficiency of replication and oncolysis of the Δ*bel2* variants (oFV-hCD19t or oFV-GFP) suggested to us that these constructs would prove to be the better oncolytics *in vivo*.

We hypothesized that we could exploit the situations where infection becomes uncoupled from oncolysis to display a CAR target antigen to confer susceptibility of infected, unlysed tumor cells to CAR T cell therapy. In this respect, Figure 2 shows that Δ*bel2* or *bel2* oFV expressing the CD19CAR target antigen conferred a *de novo* sensitivity to CAR T cell recognition and killing (Figure 2) and also led to clearance of the virus from infected cell cultures.

Using a highly sensitive 3D PCR method, we observed accumulation of G-to-A mutations in oFV-Δ*bel2* genomes with time compared with *bel2* retaining genomes, consistent with the hypothesis that retention of *bel2* expression reduced anti-viral activity of APOBEC-induced viral mutation. More surprisingly, we also observed a reproducible association of *bel2* retention with increased levels of genome deletions. As discussed above, this may be associated with the increased size of the *bel2*-retaining genomes, complications introduced into the U3 region by retention of the *bel2*-T2A-CD19 cassette and/or the possibility that *bel2* may have important undescribed properties associated with regulation of genome integrity for optimal replication.

In contrast with *in vitro* studies (Figures 1, 2, and 3), luminescence did not show a significant difference in viral infection or spread between the *bel2* retaining or deleted vectors (Figure 4) and sequencing did not show a significantly increased rate of mutation in Δ*bel2* viruses. However, consistent with the *in vitro* data, retention of *bel2* was associated with an increased frequency of deletions in the transgene.

Taking these data together, we selected the oFV-hCD19t virus for the testing of combinational *in vivo* therapy with oFV-hCD19t and CAR T cells due to the relative lack of large-scale point mutational, or deletional, loss of integrity of the genome compared with the *bel2*-retaining virus. The data of Figure 5 show that oFV-hCD19t spread efficiently *in vivo* through tumors associated with display of the CD19 CAR target antigen. However, contrary to our initial hypothesis, therapy experiments indicated that it was preferable to let infection with this slowly spreading oFV, with low level oncolytic activity, persist chronically rather than remove the infection by treatment with CD19-targeting (and therefore virus-targeting) CAR T cells (Figure 5). Thus, those mice treated with both oFV-hCD19t

and anti-CD19 CAR T cells that died earliest from tumor burden showed highly significant loss of virally infected cells (days 14–29) (Figure 5). We had proposed the combination oFV and CAR T cell therapy approach to eradicate those tumor cells which did not succumb to oncolysis despite being infected with the virus. However, the data here suggest that there was an absence of large-scale resistance to viral oncolysis despite infection which additional induced susceptibility to CAR T killing could compensate for. In addition, since we did not observe virally infected (U3-Cherry-positive) tumor cells at any significant level in CAR T treated mice that succumbed to tumor early, stability of CD19 expression must presumably have been very stably associated with virus propagation. Interestingly, these data also suggest that CAR T cell infiltration into, and through, these U251 tumors was relatively efficient since they could find and eradicate nearly all the CD19 expressing tumor cells despite the virus having a widespread distribution in non-CAR-treated tumors.

In mice that controlled tumor for longer, initial viral clearance was followed by a recurrence of the signal of viral infection (days 29–36) (Figure 5), suggesting that viral evolution was occurring *in vivo* to escape CAR T cell-mediated viral/CD19 clearance. Figure 6 provides a mechanistic explanation for this *in vivo* viral evolution to escape CAR T clearance. Virtually every viral clone analyzed from these escape tumors was unique in either point mutation load or deletion patterns. Of the 91 total clones sequenced, 90 either contained a point mutation or deletion in the T2A-hCD19t gene regions (Figures 6C–6E). The very high diversity in these oFV CAR T-escape quasi-species suggests that oFV escape from CAR T cell pressure (to remove CD19 expression) could occur in multiple ways and even that the lack of BET may provide a selective advantage to the oFV-hCD19t virus to allow for generation of mutations which can be selected for to escape CAR T cell clearance. In this respect, we did observe primarily G-to-A point mutations, which are a characteristic signature of APOBEC3 action on minus strand cDNA cytosines.[29]

Overall, the data of Figure 7 re-iterate the oncolytic activity of oFV as a single agent and also suggest that prolonged IT spread of a virus expressing a CAR target antigen may help to combine direct low level oncolysis with an additional potential therapeutic effect of added CAR T cells, although this improvement was clearly very modest (Figure 7D).

A range of different OVs has been tested in both pre-clinical and clinical studies. Differences can include genome size and form, speed of replication and the ability to carry cytotoxic or immune modulatory transgenes. Replication competent C-type retroviruses showed great promise in (fast growing) tumor models but did not fare well in human trials, although more targeted patient selection may uncover specific patient subgroups who will benefit.[16,30,31] Foamy viruses, considered to be the oldest retroviruses,[32] offer some significant differences to C-type retroviruses.[25] These include a hybrid RNA/cDNA genome and cytoplasmic latency allowing pre-integration complexes to persist until the cell divides up to 30 days p.i.[15] In addition, foamy viruses, unlike C-type retroviruses, are cytolytic in culture and oncolytic *in vivo*, which we show here induces modest, but significant, therapy as a stand-alone monotherapy. Of particular interest was the chronic presence of the virus in tumors. This contrasts with other types of OVs, such as VSV, which induce rapid replication/lysis but are generally cleared quickly by anti-viral innate responses. However, all mouse models we used so far have been immuno-compromised, and this could be a contributing factor for the chronicity. Regardless, this chronicity was attractive to use as a platform for expression of CAR target antigen to combine low level chronic oncolysis with CAR T cell therapy. However, CAR T cells were remarkably efficient at clearing oFV-infected tumor cells even within the context of a solid established tumor. Furthermore, addition of CAR T cells to the oFV infection reduced therapeutic efficacy. Therefore, our data here suggest that oFV may have significant potential as an anti-cancer agent by establishing a slow, smoldering spreading infection which is associated with low levels of oncolysis. In turn, that spread could be linked to the expression of transgene(s), which does not remove the infection (as CAR T cell targeting did here) but promotes further immune infiltration and tumor attrition. In our studies here, we used the U251 glioma cell line as a model for treatment of HGG with oFV. However, these cells still grow relatively rapidly *in vitro* and *in vivo* in mice. Therefore, testing the slowly replicating oFV in more slowly dividing tumors[33] will be important to reveal the true potential of this virus to generate long lasting infections in which the equilibrium between oncolysis and viral persistence (especially with the potential to express immune stimulating genes during persistence) can be exploited to greater effect. Comparison of fast-acting, rapidly cleared viruses with or without arming genes, with this slow-spreading, chronically signaling armed oFV will help to inform the best form of oncolytic platform for clinical development in the immune-oncology field. In addition, our data here suggest that a combination of OV platforms including oFV as one component may be of great value in future experiments. Thus, for example, early treatment with the slow, progressive oFV, may allow the clearance of a subset of susceptible tumor cells. Those tumor cells that then establish the equilibrium of lysis and persistence with the oFV may be susceptible to subsequent treatments with a different, faster acting OV which induces cell killing through different mechanisms.

In summary, we used a *bel2* deleted oFV platform to deliver a CAR target antigen to tumors. The virus persisted and spread through the tumors for long periods, while simultaneously providing a modest but significant oncolytic therapeutic benefit, suggesting the establishment of an equilibrium between viral replication and tumor cell oncolysis. *De novo* expression of a CAR target antigen was possible and efficient. However, even after long periods allowing viral spread, addition of CAR T cells decreased therapy by removing the smoldering viral infection. Our findings suggest that a modestly oncolytic, chronically persistent oFV may be a valuable platform for the chronic expression of immune activating payloads; we propose that these payloads will not necessarily induce infected cell clearance

but will be designed to allow for long term reversal of immune suppressive tumor microenvironments and immune tolerance to tumors.

MATERIALS AND METHODS

Cell lines

HEK-293T (ATCC CRL-11268; Manassas, VA, USA) were cultured in DMEM supplemented with 10% fetal bovine serum (Gibco A525670; Grand Island, NY, USA). Pediatric diffuse intrinsic pontine glioma (DIPG) SF7761 (Millipore SCC126; Burlington, MA, USA), DIPG XIII-GL (kindly proved by Dr. Dave Daniels Lab, Mayo Clinic) and the DIPG SJPDGF1 (SOH, a generous gift from Dr. Cynthia Wetmore at Phoenix Children's Hospital) were cultured in TSM media, which consists of 50% Neurobasal-A Medium (Invitrogen Cat# 10888-022; Carlsbad, CA, USA), 50% DMEM/F-12 (Invitrogen, Cat# 11330-032), 10 mM HEPES solution (Gibco, Cat# 15630-080), 1 mM MEM Sodium Pyruvate solution (Corning, 25,000-CI; Corning, NY, USA), 1× GlutaMAX Supplement (Invitrogen, Cat# 11140-050), 1× antibiotic/antimycotic solution (Invitrogen, Cat# 15240-096), 1× MEM Non-Essential Amino Acids Solution (Invitrogen, Cat# 11140-050), 1× B-27 Supplement Minus Vitamin A (Invitrogen, Cat# 12587-010), 20 ng/mL human epidermal growth factor (PeproTech, Cat# AF-100-15; Cranbury, NJ, USA), 20 ng/mL human fibroblast growth factor basic-154 (PeproTech, Cat#100-18C), 10 ng/mL human PDGF-AA (PeproTech, Cat# 100-13A), 10 ng/mL human PDGF-BB (PeptroTech, Cat# 100-14B), and 2 μg/mL heparin solution (StemCell Technologies, Cat# 7980; Seattle, WA, USA). The U251-U3-mCherry-U3-Luciferase cells and the BHK-21-U3-mCherry cells were previously reported.[11]

Foamy virus infectious clone construction

The generation of the poFV-GFP plasmid has been described previously.[10] To generate poFV-hCD19t we linearized the poFV-GFP backbone with SacII and AccIII restriction enzymes (removing T2A-GFP transgene sequence). A truncated Human CD19 (amino acids 1–332, base pairs 1–996) was generated from full-length template (NCBI: NM_001770.6) by PCR. Primers were design to include a T2A on 5′ end our hCD19t to read in-frame with *bel2* ORF immediately behind the Bel1 stop codon. Primer used were: Forward primer, tacccgcgg GAAGGACGGGGGAGCCTCCTGACATGTGGCGACGTGGAGG AGAATCCCGGACCCATGCCACCTCCTCGCCTCCTCTTCTTCC TC and reverse primer, aaatccggaTCATCTCCTGGTGGGGT CAGTCA. This was then ligated into the linearized oFV backbone via the SacII and AccIII sites. Positive clones were sent for Sanger sequencing validations (Azenta, Inc., Burlington, MA, USA). poFV-*bel2* constructs were generated from gene blocks (IDT, Integrated DNA Technologies, Coralville, IA, USA). The gene blocks were designed to clone into sites ClaI and NotI of the oFV genome. ClaI is immediately upstream of the *bel2* ATG site, and the gene block contained the full *bel2* ORF, with stop codon removed leading into a T2A sequence followed by either GFP or hCD19t genes. These gene blocks were then cut by ClaI and NotI and ligated into oFV backbone to generate either poFV-*bel2*-GFP and poFV-*bel2*-hCD19t. Again, sanger sequencing was done to confirm correctness.

Foamy virus production

HEK-293T cells were seeded in 10-cm dishes at 4e6 cells per plate and allowed overnight for additional growth and attachment. The next morning, media was replaced with fresh DMEM 10% fetal bovine serum (FBS), and cells were transfected with 15-μg of poFV plasmid mixed with 66-μl Lipofectamine 2000 (Invitrogen, Cat# 11668-500) in OptiMEM. At 48-h (day 2) after transfection, the cells were split 1:2 and transferred to 15-cm plates. At this time, we also added in 4e6 BHK-U3-mCherry cells to support the infection. At day 4 after transfection, the producer cells were again split 1:2, transferred to a new 15-cm dish and 4e6 BHK21-U3-mCherry cells were again added to the culture. On 6 day after transfection, the media containing the viral supernatant was collected, the intracellular viral particles were then released from the cells by two cycles of freezing and thawing. Finally, the virus prep was filtered through an 0.45-μm syringe filter (Millipore) and concentrated by ultracentrifugation with the SW32Ti rotor (Beckman; Brea, CA, USA) and a 20% sucrose cushion. The pellet was re suspended in PBS and stored at −80°C. Foamy viruses were titered using BHK-U3-mcherry indicator cell lines. Briefly, 100,000 cells were seeded per well of a 24-well plate. We allowed 3–4 h for cell recovery and attachment before infecting with a freshly thawed aliquot of foamy virus. Cells were infected with 10, 5, 1, or 0.1 μL of foamy virus stock. Cells were collected at 72 h p.i. for FACS analysis of live, mCherry$^+$ cells. Infectious unit (IFU) titers were calculated from wells showing $\leq$20% mCherry$^+$ cells. We took the number of cells seeded per well multiplied by percent of mCherry positive cells multiplied by the dilution factor (100,000 cells/0.20 = 20,000 IFU/1 − μL = 20,000,000 IFU/mL).

Lentivector production

Second-generation lentiviral vectors were used to transduce human T cells for the generation of CAR T cells. The following plasmids were used to generate these vectors: pHR-SIN (vector), p8.91 QV (Gag-Pol expression construct), and pMD-G (vesicular stomatitis virus glycoprotein G [VSV-G] expression construct). To produce lentivectors, low-passage HEK-293T cells were seeded at 4e6 per 10-cm dish. After overnight incubation, the media was changed to fresh growth media (DMEM, 10% FBS), and the cells were transfected with a cocktail consisting of 6 μg pHR-SIN (vector), 6 μg p8.91QV, and 1 μg pMD-G mixed with Lipofectamine 2000 (Invitrogen, Cat# 11668-500) at a 3:1 ratio in OptiMEM. Supernat was collected at 72 h after transfection, passed thru a 0.45-μm filter and concentrated down on ultracentrifuge at 47,000×*g* for 1.5 h at 4°C. The viral pellet was then gently resuspended in chilled PBS, aliquoted, and stored at −80°C. Lentivectors were titered from frozen aliquots by first seeding HEK-293T cells at 100,000 cells per well of 24-well plate. After 3–4 h, the cells were directly transduced with either 10, 5, 1, or 0.1 μL freshly thawed viral stock. After 72 h of culture, the cells were collected and FACS analyzed for GFP and scFv-CD19 (R&D Systems, Recombinant Human CD19 Protein, Atto 647N Conjugate, Cat# ATM9269).

Human CAR-T generation

Peripheral blood mononuclear cells (PBMCs) were from healthy donor apheresis cones obtained through the Mayo Clinic Blood

Donor Center (approved by the Division of Transfusion Medicine Research Committee at Mayo Clinic and determined to be Institutional Review Board exempt). PBMCs were isolated using Lympholyte-H density separation (Cedarlane, Burlington, NC, USA), aliquoted and cryopreserved (Biolife 210374; Bothell, WA, USA). To generate human CAR T-cells, total T-cells were first purified from freshly thawed vials (Miltenyi, Pan T cell Isolation Kit, Cat# 130-096-535; Gaithersburg, MD, USA). These purified T cells were cultured in RPMI containing 10% FBS, 1% penicillin/streptomycin, 1× HEPES (Gibco, Cat# 15630080), 1× sodium pyruvate (Gibco, Cat# 11360070), and 1× NEAA (Gibco, Cat# 11140050). T cells were immediately stimulated with CD3/CD28 beads (Thermo Fisher Scientific, Waltham, MA, USA; Dynabeads Human T-Activator CD3/CD28, Catalog #11131D). Twenty-four hours after stimulation with CD3/CD28, T cells were transduced at a MOI of 5 with concentrated lentiviral particles encoding a second-generation 4-1BB anti-CD19-P2A-GFP CAR construct. CAR T cells were then monitored daily, until day 5 after stimulation, where the CD3/CD28 beads were removed from the cells. From days 5 to 12 after stimulation, the CAR T-cells were counted daily and maintained at 1e6 cells/mL in CAR T growth media (recipe above). CAR T-cells were used for experiments between days 10 and 12 after stimulation CD3/CD28. CAR T cell transduction efficiency was determined at day 12, by pelleting down 1e6 cells, washing with PBS, staining with Zombie NIR Fixable Viability Kit (BioLegend, Cat# 423105; San Diego, CA, USA), and then staining with anti-human CD3 AF647 (BioLegend, Cat# 300416). Cells were FACS analysis for percent live, $CD3^+$ and GFP^+.

3D-PCR

This assay was adapted from previous publications.[34] To determine levels of mutations in oFV-GFP and oFV-*bel2*-GFP, differential DNA denaturation PCR (3D-PCR) was used, which consists of two rounds of PCR. For PCR round 1, total DNA was purified from cells using Qiagen DNeasy Blood & Tissue kit (Qiagen, Cat# 69504). We used 200 ng total DNA for normal high denaturation temperature (95°C) Ex Taq PCR (Takara, Cat# RR01AM) using the following primers against GFP: GFP-PCR1-F GTAAACGGCCACAAGTT CAG, GFP-PCR1-R CCATGTGATCGCGCTTCT. This yields a 592-bp length product. After PCR, the product was purified using Qiagen's PCR Purification Kit (Qiagen, QIAquick PCR Purification Kit, Cat# 28104) and 1 μL was used as template for PCR round 2. Again, Ex Taq polymerase was used with nested primers: GFP-PCR2-F GCTGACCCTGAAGTTCATCTG and GFP-PCR2-R CACCTTGA TGCCGTTCTTCT. Here, six independent reactions were set up per DNA sample, each reaction has a 1° decline in denaturation temperature ranging from 95°C down to 90°C. The resulting 367-bp product was fractionated on a 2% agarose gel, gel extracted and purified (Qiagen, QIAquick Gel Extraction Kit, Cat# 28706). The purified PCR products were then cloned into TOPO-TA (Invitrogen, TOPO-TA Kit, Cat# K457501). Individual clones where selected and mini-prepped (Qiagen, QIAprep Spin Miniprep Kit, Cat# 27104). Clones were sanger sequenced (Azenta) and sequences were aligned using DNA Dynamo Software (Blue Tractor Software Ltd. Wales, UK).

Complete Amplicon-EZ sequencing

The following methods were used under guidance from Azenta Inc. Primers were generated to a 450-bp fragment of hCD19t gene of our oFV vectors. For Amplicon sequencing, Illumina adapters were added to each end of the primers. Primers used were: Primer-CD19-F acactctttccctacacgacgctcttccgatctATGCCACCTCCTCGCC TCCTCTTCTTCCTC and Primer-CD19-R gactggagttcagacgtgtg ctcttccgatctCTTCCCGGAAGGGGAGCTGGGGCCCTCTGA with Illumina adapters in lowercase. PCR was conducted using high fidelity KOD Hot Start DNA polymerase (Sigma-Aldrich, St Louis, MO, USA; Cat# 71086). PCR products were then gel extracted and purified (Qiagen, QIAquick Gel Extraction Kit, Cat# 28706), DNA concentration was normalized to 500 ng/25 μL volume using QUANT-IT PICOGREEN (Invitrogen, Cat# P11496). Samples were then sent to Azenta for Complete Amplicon-EZ sequencing and analysis. All sequences obtained that were greater than 1% frequency were included in data; everything less than 1% was considered a background error.

In vivo experiments

All *in vivo* experiments were approved and monitored by the Mayo Clinic's Institutional Animal Care and Use Committee. For all *in vivo* experiments we used 6-week-old female NSG (NOD.Cg-Prkdcscid Il2rgtm1Wjl/SzJ, Strain 005557) from The Jackson Laboratory (The Jackson Laboratory, Bar Harbor, ME, USA). *In vivo* spread of a CAR target antigen by oFV (Figure 4) experiments, NSG mice were challenged subcutaneously with 5×10^6 U251-U3-mCherry-U3-F.Luc cells in 100-μL of PBS (Hyclone). When tumors reached the volume of 0.3–0.5 cm^3, tumors were directly injected with two doses of either PBS, 5×10^5 IU oFV-hCD19t or 5×10^5 IU oFV-*bel2*-hCD19t (n = 3/group). oFV infection and expression was then assessed on days 9 and 16 p.i. by bioluminescence imaging with IVIS Lumina X5 imaging system after an intraperitoneal injection of D-luciferin (20 mg/mL [Gold Biotechnology, Olivette, MP, USA; D-Luciferin potassium salt, Cat# Luck-1G). At endpoint, tumors from PBS- and oFV-treated mice were harvested after euthanasia and divided into two parts: one-half was explanted and immediately fixed in 4% PFA for confocal analysis (Santa Cruz Biotechnology, Dallas, TX, USA; paraformaldehyde solution 4% in PBS, Cat# sc-281692) overnight at 4°C. After fixing, tumors were soaked in 15% and 30% sucrose solution before mounting in OCT (Tissue-Tek, O.C.T. Compound, Cat# 4583) embedding mount and flash frozen. Cryosections were made at 6 μm. A portion of the other half of tumor was snap frozen and stored at −80°C until genomic DNA was isolated with the DNeasy Blood and Tissue kit (Qiagen).

For *in vivo* experiments, oFV delivering CAR T cell target to tumors (Figure 5), NSG mice were again challenged subcutaneously with 5×10^6 U251-U3-mCherry-U3-F.Luc cells in 100 μL PBS (Hyclone). When tumors reached the volume of 0.3–0.5 cm^3, tumors were directly injected with one dose of either PBS, 3.3×10^6 IU, 6.6×10^6 IU, or 1×10^7 IU of oFV-hCD19t (n = 8/group). oFV infection and expression was then assessed weekly by bioluminescence imaging with IVIS Lumina ×5 imaging system after an intraperitoneal injection of D-luciferin (20 mg/mL [Gold Biotechnology]). On day

Table 1. Primer and probe sequences used in qPCR reaction

Primer name	Sequence
oFV ENV QPCR F	GTCACTCAGAGGGCTGTTTATC
oFV ENV QPCR R	CTTGTGGGATACTGGTCATGT
oFV ENV QPCR Probe	/56-FAM/CGTTCCCTT/ZEN/ AGAGTGCAACACCCA/3IABkFQ/
T2A-hCD19_QPCR_F primer	CCTGACATGTGGCGACG
T2A-hCD19_QPCR_R primer	AAGAGGAGGAAGAAGAGGAGG
T2A-hCD19_QPCR_Probe	TCCGGGATTCTC
ActB Human QPCR PROBE/PRIMER	Hs.PT.39a.22214847

11 p.i., mice received a single intravenous injection of either UTD human T cells or anti-CD19-P2A-GFP CAR T cells (5×10^6 cells/mouse). At point, tumors from PBS- and oFV-treated mice were harvested after euthanasia and divided into two parts: one-half fixed in 4% PFA for confocal analysis (more detail above), the other tumor half was minced and incubated with Liberase TL (Roche, Basel, Switzerland) and deoxyribonuclease I (DNase I) (Sigma-Aldrich) for 30 min at 37°C. Up to 30 mg of tumor was stained and run on the flow cytometer. Again, a small portion of tumor was snap frozen for DNA extraction. The survival endpoint was reached when the tumor size reached 1.2 cm in diameter. Tumor volume was calculated as follows: Volume = $(\text{Length} \times \text{Width}^2)^2$.

For *in vivo* experiments, longer viral spread minimally enhances CAR T therapy (Figure 7). Methods are identical to above; however, control mice received oFV-GFP (1e7 IU/mouse). All oFV-treated mice then received anti-CD19-P2A-GFP CAR T-cells (5 × 106 cells/mouse) on day 35 p.i. with oFV. Tumors were allowed to grow until they reached point conditions based on the tumor size (>10% body weight) or body scoring condition and were euthanized.

Flow cytometry

Flow cytometry was performed on cell lines or freshly explanted tumors or spleens. For tumors, tumors were first weighed then minced and incubated with Liberase TL (Roche) and deoxyribonuclease I (DNase I) (Sigma-Aldrich) for 30 min at 37°C. Roughly 30 mg of single cell suspensions were first washed with PBS, centrifuged down and the resulting pellet was resuspended with Zombie NIR (Biolegend, Zombie NIR Fixable Viability Kit, Cat#423106). After incubation, cells were again pelleted by centrifuge and washed with FACS buffer (PBS +1% BSA), and pelleted down again. Tumors were then stained with anti-human CD3-AF647 (Biolegend, Cat# 300416). After staining, cells were washed with FACS buffer 2× then fixed with 4% formaldehyde buffer. Cells were analyzed using ZE5 Cell Analyzer using Everest v2.0 software in the Mayo Clinic Flow Cytometry Core. Data were analyzed using FlowJo version 10.5.

qPCR assays

Genomic DNA was extracted using Qiagen DNeasy Blood & Tissue kit (Qiagen, Cat# 69504). DNA was nano-dropped (Thermo Fisher Scientific) and normalized to 20 ng/μL. We used 5 μL of this DNA per Q-PCR reaction with a 2× PrimeTime Gene Expression Master Mix (Integrated DNA Technologies, Coralville, IA, USA; Cat# 1055772). Primer and probe sequences are shown in Table 1.

Immunohistochemistry

Cryopreserved tumors were sections on cryostat to 6-μm sections. Sections were washed in PBS (HyClone), permeabilized with 0.3% Triton X-100 (Sigma) and blocked in 5% FBS PBS solution. Sections were stained for either anti-CD19-AF647 (Biolegend, Cat# 302212, 1:100 dilution) or anti-CD3-AF647 (Biolegend, Cat# 300416, 1:100 dilution) overnight at 4C. Nuclei were stained with DAPI solution (Invitrogen, Cat# D1306). The sections were imaged using a Zeiss LSM 780 confocal microscope and analyzed with the Zen software.

Bioluminescent assay

These assays utilize the foamy virus U3 promoter driving firefly luciferase reporter (U3-F.Luc). U251-U3-F.Luc cells were seeded at 10,000 cells/well in a 96-well black plate (Thermo Fisher Scientific, Cat# 165305). At 6 h after seeding, cells were infected with respective oFVs at a MOI of 1. At 72 h p.i., conditioned media was carefully removed and CD19 CAR-Ts or UTD T cells were added at indicated ratios in 200-μL CAR T cell growth media (recipe above). The reaction was allowed 24 h co-culture before reading on a luminometer. For luminescence reading, One Glo Ex Luciferase substrate (Promega, Madison, WI, USA; Cat# E8130) was added based on manufacturers protocol. Briefly, the 96-well plate was centrifuged gently at 1,200 rpms, then 100 μL of conditioned CAR T cell media was removed and saved for Human IFN-γ ELISA. To the remaining 100 μL, One Glo Ex luciferase substrate was added, gently mixed, incubated for 5 min, and then luminescence was read on luminometer. For DIPG SOH and SF7761, cells were seeded at 50,000 cells per well in 96-well black plate (Thermo Fisher Scientific). These cells were infected at MOI 1 with indicated oFVs. After 72 h, CD19 CAR-T were added at indicated effector to target ratios. Co-culture was allowed 24 h before reading luminescence. Human IFN-γ production measured by ELISA in conditioned media after 24 h of co-culture with each indicated oFV-infected U251-U3 cells and CAR-Ts or UTD T-cells (R&D Systems, Cat# DY285B).

Statistical analysis

All statistical analyses were done using GraphPad Prism 8, with tests specified in figure legends and alpha = 0.05.

Diagrams

Diagrams were created with https://www.BioRender.com.

DATA AND CODE AVAILABILITY

The authors confirm that the data supporting the findings of this study are present within the article.

SUPPLEMENTAL INFORMATION

Supplemental information can be found online at https://doi.org/10.1016/j.omton.2024.200852.

ACKNOWLEDGMENTS

The authors thank Toni L. Woltman for expert secretarial assistance. Funding provided by the National Institutes of Health (R21CA262994; R01AI170535-01; R01 CA269384-01; P50 CA210964), The Richard M. Schulze Family Foundation, Mayo Foundation, and a research grant from Vyriad, Inc.

AUTHOR CONTRIBUTIONS

J.M.T. conducted experiments and writing original draft. K.B. conducted experiments and edited paper. T.F.C. conducted experiments and edited paper. L.E. conducted experiments. J.T. data collection. R.B. data collection. B.K. data analysis. R.M.D. provided supervision and project administration. S.J.R. provided supervision and funding acquisition. R.G.V. provided supervision, funding acquisition, editing paper, investigation, and visualization.

DECLARATION OF INTERESTS

R.V. was a recipient of a research grant from Vyriad Inc.

REFERENCES

1. June, C.H., and Sadelain, M. (2018). Chimeric antigen receptor therapy. N. Engl. J. Med. *379*, 64–73.
2. Petersen, C.T., and Krenciute, G. (2019). Next Generation CAR T Cells for the Immunotherapy of High-Grade Glioma. Front. Oncol. *9*, 69.
3. Antonucci, L., Canciani, G., Mastronuzzi, A., Carai, A., Del Baldo, G., and Del Bufalo, F. (2022). CAR-T Therapy for Pediatric High-Grade Gliomas: Peculiarities, Current Investigations and Future Strategies. Front. Immunol. *13*, 867154.
4. Prapa, M., Chiavelli, C., Golinelli, G., Grisendi, G., Bestagno, M., Di Tinco, R., Dall'Ora, M., Neri, G., Candini, O., Spano, C., et al. (2021). GD2 CAR T cells against human glioblastoma. NPJ Precis. Oncol. *5*, 93.
5. Watanabe, N., McKenna, M.K., Rosewell Shaw, A., and Suzuki, M. (2021). Clinical CAR-T Cell and Oncolytic Virotherapy for Cancer Treatment. Mol. Ther. *29*, 505–520.
6. Park, A.K., Fong, Y., Kim, S.I., Yang, J., Murad, J.P., Lu, J., Jeang, B., Chang, W.C., Chen, N.G., Thomas, S.H., et al. (2020). Effective combination immunotherapy using oncolytic viruses to deliver CAR targets to solid tumors. Sci. Transl. Med. *12*, eaaz1863.
7. Liu, Y., Zheng, Y., Deng, T., Huang, Y., Liu, Z., Zhan, B., Zhou, X., Yan, R., Ren, J., Xing, Y., et al. (2022). Oncolytic herpes simplex virus delivery of dual CAR targets of CD19 and BCMA as well as immunomodulators to enhance therapeutic efficacy in solid tumors combined with CAR T cell therapy. Front. Oncol. *12*, 1037934.
8. Aalipour, A., Le Boeuf, F., Tang, M., Murty, S., Simonetta, F., Lozano, A.X., Shaffer, T.M., Bell, J.C., and Gambhir, S.S. (2020). Viral Delivery of CAR Targets to Solid Tumors Enables Effective Cell Therapy. Mol. Ther. Oncolytics *17*, 232–240.
9. Tang, X., Li, Y., Ma, J., Wang, X., Zhao, W., Hossain, M.A., and Yang, Y. (2020). Adenovirus-mediated specific tumor tagging facilitates CAR-T therapy against antigen-mismatched solid tumors. Cancer Lett. *487*, 1–9.
10. Budzik, K.M., Nace, R.A., Ikeda, Y., and Russell, S.J. (2021). Oncolytic Foamy Virus - generation and properties of a nonpathogenic replicating retroviral vector system that targets chronically proliferating cancer cells. J. Virol. *95*, e00015-21.
11. Budzik, K.M., Nace, R.A., Ikeda, Y., and Russell, S.J. (2022). Evaluation of the stability and intratumoral delivery of foreign transgenes encoded by an oncolytic Foamy Virus vector. Cancer Gene Ther. *29*, 1240–1251.
12. Mergia, A., Leung, N.J., and Blackwell, J. (1996). Cell tropism of the simian foamy virus type 1 (SFV-1). J. Med. Primatol. *25*, 2–7.
13. Phung, H.T.T., Tohya, Y., Shimojima, M., Kato, K., Miyazawa, T., and Akashi, H. (2003). Establishment of a GFP-based indicator cell line to quantitate feline foamy virus. J. Virol. Methods *109*, 125–131.
14. Maetzig, T., Galla, M., Baum, C., and Schambach, A. (2011). Gammaretroviral vectors: biology, technology and application. Viruses *3*, 677–713.
15. Lehmann-Che, J., Renault, N., Giron, M.L., Roingeard, P., Clave, E., Tobaly-Tapiero, J., Bittoun, P., Toubert, A., de Thé, H., and Saïb, A. (2007). Centrosomal latency of incoming foamy viruses in resting cells. PLoS Pathog. *3*, e74.
16. Hogan, D.J., Zhu, J.J., Diago, O.R., Gammon, D., Haghighi, A., Lu, G., Das, A., Gruber, H.E., Jolly, D.J., and Ostertag, D. (2018). Molecular Analyses Support the Safety and Activity of Retroviral Replicating Vector Toca 511 in Patients. Clin. Cancer Res. *24*, 4680–4693.
17. Hooks, J.J., and Gibbs, C.J., Jr. (1975). The foamy viruses. Bacteriol. Rev. *39*, 169–185.
18. Matsen, F.A., 4th, Small, C.T., Soliven, K., Engel, G.A., Feeroz, M.M., Wang, X., Craig, K.L., Hasan, M.K., Emerman, M., Linial, M.L., and Jones-Engel, L. (2014). A novel Bayesian method for detection of APOBEC3-mediated hypermutation and its application to zoonotic transmission of simian foamy viruses. PLoS Comput. Biol. *10*, e1003493.
19. Rua, R., Betsem, E., and Gessain, A. (2013). Viral latency in blood and saliva of simian foamy virus-infected humans. PLoS One *8*, e77072.
20. Murray, S.M., Picker, L.J., Axthelm, M.K., Hudkins, K., Alpers, C.E., and Linial, M.L. (2008). Replication in a superficial epithelial cell niche explains the lack of pathogenicity of primate foamy virus infections. J. Virol. *82*, 5981–5985.
21. Beard, B.C., Keyser, K.A., Trobridge, G.D., Peterson, L.J., Miller, D.G., Jacobs, M., Kaul, R., and Kiem, H.P. (2007). Unique integration profiles in a canine model of long-term repopulating cells transduced with gammaretrovirus, lentivirus, or foamy virus. Hum. Gene Ther. *18*, 423–434.
22. Delebecque, F., Suspène, R., Calattini, S., Casartelli, N., Saïb, A., Froment, A., Wain-Hobson, S., Gessain, A., Vartanian, J.P., and Schwartz, O. (2006). Restriction of foamy viruses by APOBEC cytidine deaminases. J. Virol. *80*, 605–614.
23. Hamann, M.V., and Lindemann, D. (2016). Foamy Virus Protein-Nucleic Acid Interactions during Particle Morphogenesis. Viruses *8*, 243.
24. Jaguva Vasudevan, A.A., Becker, D., Luedde, T., Gohlke, H., and Munk, C. (2021). Foamy Viruses, Bet, and APOBEC3 Restriction. Viruses *13*, 504.
25. Schmidt, M., and Rethwilm, A. (1995). Replicating foamy virus-based vectors directing high level expression of foreign genes. Virology *210*, 167–178.
26. Schwantes, A., Ortlepp, I., and Löchelt, M. (2002). Construction and functional characterization of feline foamy virus-based retroviral vectors. Virology *301*, 53–63.
27. Suspene, R., Henry, M., Guillot, S., Wain-Hobson, S., and Vartanian, J.P. (2005). Recovery of APOBEC3-edited human immunodeficiency virus G->A hypermutants by differential DNA denaturation PCR. J. Gen. Virol. *86*, 125–129.
28. Saib, A., Koken, M.H., van der Spek, P., Peries, J., and de The, H. (1995). Involvement of a spliced and defective human foamy virus in the establishment of chronic infection. J. Virol. *69*, 5261–5268.
29. Harris, R.S., Bishop, K.N., Sheehy, A.M., Craig, H.M., Petersen-Mahrt, S.K., Watt, I.N., Neuberger, M.S., and Malim, M.H. (2003). DNA deamination mediates innate immunity to retroviral infection. Cell *113*, 803–809.
30. Huang, T.T., Hlavaty, J., Ostertag, D., Espinoza, F.L., Martin, B., Petznek, H., Rodriguez-Aguirre, M., Ibañez, C.E., Kasahara, N., Gunzburg, W., et al. (2013). Toca 511 gene transfer and 5-fluorocytosine in combination with temozolomide demonstrates synergistic therapeutic efficacy in a temozolomide-sensitive glioblastoma model. Cancer Gene Ther. *20*, 544–551.
31. Perez, O.D., Logg, C.R., Hiraoka, K., Diago, O., Burnett, R., Inagaki, A., Jolson, D., Amundson, K., Buckley, T., Lohse, D., et al. (2012). Design and selection of Toca 511 for clinical use: modified retroviral replicating vector with improved stability and gene expression. Mol. Ther. *20*, 1689–1698.
32. Rethwilm, A., and Bodem, J. (2013). Evolution of foamy viruses: the most ancient of all retroviruses. Viruses *5*, 2349–2374.
33. Dasgupta, P., Balasubramanyian, V., de Groot, J.F., and Majd, N.K. (2023). Preclinical Models of Low-Grade Gliomas. Cancers *15*, 596.
34. Suspene, R., Aynaud, M.M., Guetard, D., Henry, M., Eckhoff, G., Marchio, A., Pineau, P., Dejean, A., Vartanian, J.P., and Wain-Hobson, S. (2011). Somatic hypermutation of human mitochondrial and nuclear DNA by APOBEC3 cytidine deaminases, a pathway for DNA catabolism. Proc. Natl. Acad. Sci. USA *108*, 4858–4863.